POLITECNICO DI TORINO

POLITECNICO DI TORINO

Master Degree course in Ingegneria Energetica e Nucleare (LM-30)

Master Degree Thesis

Analysis and Feasibility Study of a Parabolic Solar Concentration System Installed on the Roof of the Energy Center Utilizing Organic Rankine Cycle

Supervisors
Prof. Davide PAPURELLO

Candidate
Giuseppe Davide GITTO

ACADEMIC YEAR 2023-2024

Acknowledgements

Abstract

The thesis study focuses on the analysis and feasibility of powering an Organic Rankine Cycle (ORC) with an electrical power production of 10 kW, driven by a parabolic trough Concentrated Solar Power (CSP) plant. The reference plant is the parabolic reflector installed on the roof of the Energy Center at the Polytechnic University of Turin.

After focusing on global energy demand and the limits set in recent years, this study describes the fundamental elements of concentrated solar technology, addressing its state of the art and applications.

Leading up to the thesis work, the functioning and operation of storage systems were discussed, given the unpredictability of the solar renewable source. This concluded with the description of the Organic Rankine Cycle and the potential plant strategies for energy production. ORC is a conventional Rankine Cycle driven by organic compound as working fluid instead of water, and it is particularly appropriate for low temperature applications. Different influences were studied based on the type of fluid, with a greater focus on single-cycle and regenerative plant strategies.

The ORC cycle and then the parabolic collector are sized according to the electric power produced and the choice of the organic fluid. For the sizing of the Organic Rankine Cycle, the plant is built on the ASPEN PLUS software that allow to schematize it in both simple and regenerative configurations. Through its use, the report focuses on presenting and discussing operational differences under vary conditions and optimal operating points, within critical operational limits.

Simulation results have therefore allowed to demonstrate the feasibility of the plant and to discuss its potential.

Contents

Nomenclature

A_a	Aperture area
A_f	Geometric factor
A_r	Receiver area
A_{dish}	Dish Area
$A_{slarfield}$	Solar field area
C	Concentration ratio
C_R	Geometric concentration ratio
$C_{R,o}$	Optical concentration ratio
C_{el}	Cost of electric energy
C_p^0	Purchasing cost to base conditions
C_{th}	Cost of thermal energy
E	Energy of a photon
E_{CHP}	Electric energy by cogeneration
$F(\lambda)$	Spectral Irradiance
F_M	Material factor
F_P	Pressure Factor
F_{BM}	Bare Module Factor
F_{CHP}	Fuel energy by cogeneration
$F_{s,c}$	View factor between sky and collector's surface
H	Total power density
H_0	Solar irradiance

H_{CHP} Thermal energy by cogeneration

H_{melt} Melting Enthalpy

H_{sun} Solar power density at the Sun's surface

I_a Flux incident on the aperture

I_c Solar radiation incident on the collector

I_h Total solar radiation received by an horizontal surface

I_r Solar flux received by the absorber

I_t Total radiation

$I_{b,c}$ Direct beam radiation on collector's surface

$I_{b,n}$ Normal beam radiation

$I_{d,c}$ Diffuse sky radiation on collector's surface

$I_{d,h}$ Horizontal diffuse radiation

$I_{r,c}$ Reflected solar radiation from the ground

J Joule

K Kelvin degree

KNO_3 Potassium Nitrate

KWh Kilo Watt per hours

MW_e Mega Watt electrics

N_aNO_3 Sodium Nitrate

N_c Number of collectors

N_u Nusselt number

P Pressure

P_r Prandtl number

$P_{el,t}$ Electric power of the Turbine

$P_{th,cond}$ Thermal power of the Condenser

Q Heat

Q_{cond} Condenser power

Q_{csp}	Power produced by the solar collector
Q_{eva}	Evaporator power
Q_{liq}	Sensible heat to liquid state
Q_{melt}	Latent heat
Q_{reg}	Regenerator power
Q_{sol}	Sensible heat to solid state
R_{sun}	Radius of the Sun
T	Temperature
T_a	Ambient temperature
T_c	Temperature of cold states
T_h	Temperature of hot states
T_r	Collector temperature
U_c	Overall heat loss coefficient
W_p	Pump power
W_t	Turbine power
W_{net}	Net power
α	Absorptance
α	Solar altitude angle
β	Tilt angle
$\dot{m}$	Mass flow rate
ϵ	Emittance
η_b	Efficiency of basic Rankine cycle
η_c	Collector efficiency
η_o	Optical efficiency
η_p	Pump efficiency
η_r	Efficiency of regenerative Rankine cycle
η_r	Regenerator efficiency

$\eta_{E,RIF}$ Average convetional efficiency of the Italian electricity generation fleet

$\eta_{T,RIF}$ Average conventional efficiency of the Italian thermal generation fleet

η_{cog} Cogeneration efficiency

η_{el} Electrical efficiency

η_{orc} Organic Rankine Cycle efficiency

$\eta_{t,is}$ Isentropic turbine efficiency

λ Wavelenght

μ Relative viscosity

ϕ Photon flux

ρ Densities

ρ Reflectance

σ Stefan-Boltzmann constant

τ Transmittance

θ_m Half acceptance angle

θ_{max} Maximum temperature state

θ_{min} Minimum temperature state

ξ Degree of wetness or dryness of a fluid

a_w Azimut angle

c Speed of light

c_p Specific heat capacities

d Dimension term

eV Electron Volt

f Friction factor

f_u Storage material utilisation coefficient

h Heat transfer coefficient

h Planck's constant

h_{ann} Annual hours of operation

i Angle of incidence

k Conductivity

m Mass

q_u Useful energy delivered by a collector

s Mass Entropy

u Velocity

AACE Advancement of Cost Engineering International

ALT Atmospheric Lifetime

ASHRAE American Society of Heating, Refrigerating and Air Conditioning Engineers

AU Astronomical Unit

B.C Before Christ

BEC Bare Erected Cost

CAR High Efficiency Cogeneration

CB Certificati Bianchi

CEPCI Chemical Engineering Plant Cost Index

CHP Combined Heat and Power

CSP Concentrating Solar Power

D.M Ministerial decree

DNI Direct Normal Irradiation

DSG Direct Steam Generation

EPCC Engineering, Procurement, and Construction Cost

FPC Flat Plate Collector

FR Fresnel Reflector

GSE Gestore dei Servizi Energetici

GWP Global Warming Potential

HCS Hydro Carbons

HFC Hydro Fluoro Carbons

HT High Temperature

HTF Heat Transfer Fluid

I Investment cost

i Discount rate

IAU International Astronomical Unit

LCOE Levelised Cost of Electricity

LFR Linear Fresnel Reflector

LLC Lower Limit Curve

LT Low Temperature

MTOE Million Tons of Oil Equivalent

NCF Net Cash Flow

NETL National Energy Technology laboratory

NPV Net Present Value

NZE Net Zero Emissions

ODP Ozone Depletion Potential

ORC Organic Rankine Cycle

PBT Pay Back Time

PCM Phase Change Material

PT Parabolic Trough

PV Photovoltaics

R&D Research and Development

RE Renewable Energy

RISP Primary energy saving

S Savings

SD Solar Dish

SRC Supercritical Rankine Cycle

ST Solar Tower

TASC Total As-Spent Capital

TEE Titoli di Efficienza Energetica

TEP Tonnellata Equivalente di Petrolio

TLC Trilateral Cycles

TOC Total Overnight Capital

TOE Tons of Oile Equivalent

TPC Total Plant Cost

ULC Upper Limit Curve

Chapter 1

Introduction to Solar Energy Conversion

"A thing that will assume enormous importance quite soon is the exhaustion of our fuel resources. Coal and oil have been accumulating on the earth for over five hundred million years, and at the present rates of demand for mechanical power, the estimates are that oil will be all gone in about a century, and coal probably in a good deal less than five hundred years. For the present purpose, it does not matter if these are under-estimates; they could be doubled or trebled and still not affect the argument. Mechanical power comes from our reserves of energy, and we are squandering our energy capital quite recklessly. It will very soon be all gone, and in the long run, we shall have to live from year to year on our earnings. All the energy from coal and oil came from the conversion of the energy of sunlight into the chemical energy contained in plants;" (Charles Galton Darwin 1953 The Next Million Years).

Fossil fuels can be seen as a reservoir of stored solar energy, essentially representing our energy savings or capital. In addition to these, we also have access to other forms of energy derived indirectly from the sun, such as wind, biomass, ocean, and hydropower, as well as geothermal and nuclear energy sourced from radioactive materials. What's evident is that, over the past century, we've been depleting our energy reserves, using them at unsustainable rates, while neglecting to fully harness our direct and ongoing source of energy: the sun. [27]

1.1 Global Energy Needs

Global energy consumption has experienced rapid growth over the past 50 years, and this trend is expected to continue. However, there are some significant differences between the two periods. The previous surge in energy consumption was driven by the availability of relatively cheap fossil fuels and increased industrialization in North America, Europe, and Japan. While energy consumption continues to rise in these regions, several additional factors make the energy landscape for the next 50 years more complex.

These complicating factors include the rapid growth in energy demand in China and India, which represent a significant portion of the world's population. Additionally, concerns about the imminent depletion of oil resources and the impact of human activities on global climate change

add complexity to the energy outlook. On a positive note, renewable energy technologies like wind, biofuels, solar thermal, and photovoltaics (PV) are showing maturity and the potential for cost competitiveness.

From 1971 to 2002, global primary energy demand increased from 5536 million tons of oil equivalent (MTOE) to 10,345 MTOE, with an average annual growth rate of 2%. By 2008, this demand had risen to 12,271 MTOE, indicating an average annual increase of about 3%, primarily due to the escalating energy demand in the Asia Pacific region, particularly in China. Since energy consumption per capita in highly populated countries like China and India remains relatively low, there is the possibility of sustained high growth in global energy use.

However, since 2008, the average annual energy consumption increase has dropped to approximately 2.1%, mainly because of the economic recession in the United States and Europe, where energy use decreased. Even with a 2% annual increase, the primary energy demand in 2008 (12,271 MTOE) would double by 2043 and triple by 2063, showing that global energy consumption cannot continue to grow at the same pace indefinitely.

Given this context, it becomes clear that a significant portion of the global energy demand in 2050, potentially up to 50%, must come from renewable energy sources, with solar energy and wind playing a significant role. To meet the future energy requirements for buildings, food production, water supply, transportation, industry, and electrical power, it is crucial to assess the availability and capacity of renewable energy resources. [9].

1.1.1 Global Energy Transition

The shift towards clean energy is gaining momentum globally. This shift is driven by policy initiatives, technological advancements, and economic considerations. The need to reduce greenhouse gas emissions urgently is widely recognized in response to mounting evidence of global climate change. This urgency is reflected in increasingly ambitious national objectives.

As of the end of November 2022, 87 countries and the European Union have committed to achieving net-zero emissions during this century. These commitments collectively encompass more than 85% of the world's emissions and 85% of its gross domestic product. Over the past decade, there has been a rapid increase in the adoption of clean energy technologies. The supply of energy from non-fossil sources has surged, particularly renewables. In 2022, renewables contributed to 30% of global power generation, up from less than 20% in 2010. This increase has been particularly notable in solar photovoltaic, wind, hydropower, and bioenergy production. Electrification is also gaining traction across various sectors.

The rapid expansion of solar and wind power, the increasing popularity of electric vehicles, and the adoption of various technologies for different types of production are characterized by the emergence of a new global energy economy. As this transition unfolds, it is also impacting the industries involved in the production of materials and products essential to the energy system. This marks the beginning of a new era in industry, often referred to as the "age of clean energy technology manufacturing."

Leading economies across the globe, spanning Asia, Europe, and North America, are intensifying their initiatives to enhance the production of clean energy technologies. Their objectives include advancing the transition to net-zero emission, reinforcing energy security, and remaining competitive in the evolving energy landscape. The current global energy crisis has expedited these efforts further.

These developments mean a lot, not only for the citizens around the world but for governments and investors too. Every nation must determine how it can take advantage of the opportunities and address the challenges presented by this emerging energy economy.

Investment in clean energy technology is on the rise, surpassing USD 3.4 trillion in 2022. This accounts for nearly 70% of the year-on-year growth in overall energy investment, up from approximately USD 1 trillion in 2015. In 2022, renewables, power grids, and energy storage represented more than 80% of total power sector investment, with solar photovoltaics taking the lead. This is a significant increase from 2015 when renewables comprised 75% of the $315 billion invested, while the share of fossil fuel power dropped from around 20% to 10% during the same period. [3].

1.1.2 Fossil fuels continue to be a dominant source of energy worldwide

Despite the rapid growth in clean energy technologies in recent years, the world's primary energy supply continues to be heavily reliant on fossil fuels(Figure 1.1).

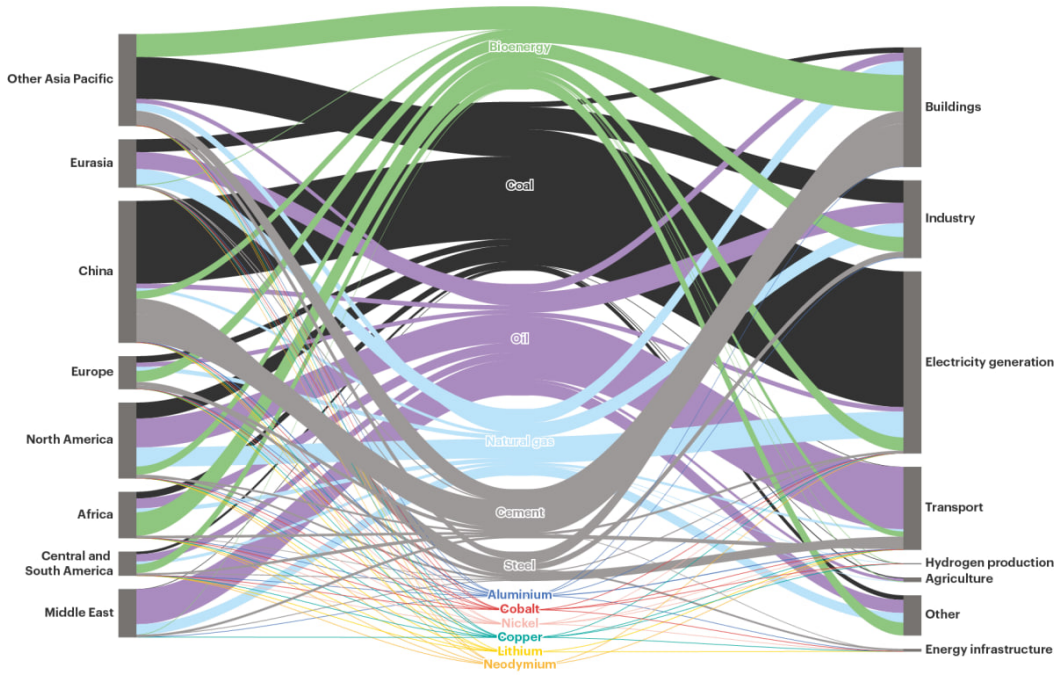

Figure 1.1: Physical mass flows of fuels and materials in the energy system in a million tonnes.

The expansion of oil, gas, and coal industries, especially in emerging and developing economies, has outpaced the growth in clean energy sources since 2000. In these countries, the share of fossil fuels in their total primary energy supply has increased from 77% in 2000 to 80% in 2021, primarily due to a significant rise in coal consumption, from 27% to 35%. In advanced economies, the share of fossil fuels decreased from 82% to 77% over the same period. Consequently, the overall contribution of fossil energy to the global energy mix has remained relatively stable at around 80%.

Additionally, apart from the direct use of energy, various end-use sectors consume substantial amounts of energy embedded in materials. This includes materials like cement for construction and infrastructure, steel for vehicles and manufacturing, and chemicals for fertilizers and consumer goods. The production of these bulk materials is predominantly reliant on fossil fuels, either for combustion or as a source of feedstock. In 2021, coal played a role in approximately 75% of the energy used in global steel production and over half of the energy used in cement production. About 70% of chemical production was based on oil or natural gas.

The demand for "critical minerals," used to produce metals like copper, nickel, and cobalt, has surged in recent years, driven by the proliferation of clean energy technologies, particularly batteries. However, the combined production of these critical minerals by mass represents only 0.3% of that of coal. Currently, the extraction and processing of critical minerals often rely on fossil fuels [3].

1.1.3 Clean Energy for Net Zero

Reaching the goal of achieving global net-zero carbon dioxide emissions by 2050 necessitates not only reducing the growth in energy demand but also making a profound transformation in the energy sources and technologies we rely on (Figure 1.2).

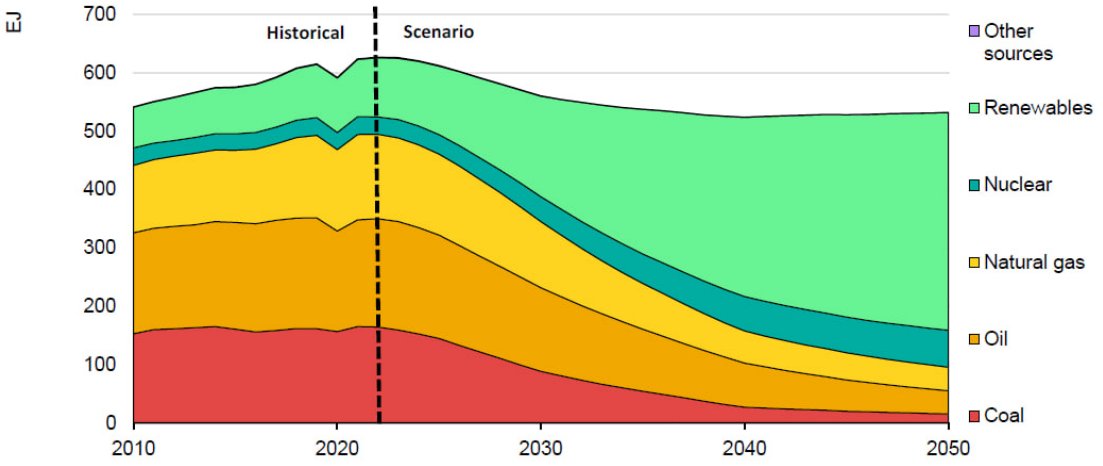

Figure 1.2: Global total primary energy supply in the NZE Scenario [3]

In the Net Zero Emissions (NZE) Scenario, behavioral changes, enhanced energy efficiency, and a shift towards renewables contribute to a 10 percent decrease in total primary energy supply until 2030, despite the global economy expanding by nearly one-third. The focus shift to the drops of 9 percent in the total final consumption in the same period, and in the annual rate of improvement in energy efficiency that increases significantly nearly tripling over 4 percent per year compare to the previous decade. From 2030 to 2050, global energy demand experiences a slower decline, decreasing by a 15 percent in total, as the potential for further energy conservation and efficiency gains decrease, while a growing population and economic activity continue to drive up the fundamental need for energy services. Clearly the renewables energy, especially solar PV ad wind power, show the biggest supply increase in the NZE Scenario respect to 2050, followed

by a significant increase for the Nuclear power too. These developments will lead to doubling the electricity demand, that becomes the mainly energy vector reaching more than half of total final consumption in 2050 (fig2). Then the total electricity generation grows by 3.5% per year to 2050 in order to meet that demand.

Actually, a significant portion of the clean energy technologies needed to achieve a net-zero emissions status by the middle of this century are currently not available at a large scale. Although the emissions reduction required by 2030 in the Net Zero Emissions (NZE) Scenario can be accomplished using existing technologies or that are well known. Approximately half of the emissions reductions projected for 2050 will rely on technologies that are currently in the prototype or demonstration phases [3].

1.2 Solar Energy

Harnessing solar energy for effective heating has a long history dating back to ancient times. In 213 B.C., the Greek scholar Archimedes famously used mirrors to concentrate sunlight onto the fleet of Marcellus, a Roman general who sought to capture Syracuse (Sicily). This clever application set the Roman ships ablaze. Interestingly, today's solar devices aren't necessarily more advanced than those employed by Archimedes.

The current landscape of solar energy technology reflects significant advancements. Commercial solar panel efficiencies have now surpassed 20%, while in laboratories, multi-junction solar cells operating under concentrated sunlight have achieved efficiencies exceeding 40%. Solar thermal systems also exhibit notable efficiencies ranging from 40% to 60%.

Solar thermal power, which employs concentrating solar collectors, was the earliest solar technology to demonstrate its potential for grid-scale power generation. Notably, a 354-megawatt electric (MWe) concentrating solar thermal power (CSP) plant has been in continuous operation in California since 1988. However, progress in the field of solar thermal power encountered challenges in subsequent years due to inadequate policy support and a lack of research and development (R&D) efforts.

In recent years, there has been a resurgence of interest in solar thermal power, with various solar thermal power plants now under construction worldwide. This renewed focus underscores the growing recognition of solar thermal power's potential as a sustainable and reliable source of electricity, particularly in the context of increasing global attention to renewable energy and the reduction of greenhouse gas emissions [27].

1.2.1 Thermal Conversion

Thermal conversion is an engineering process that leverages a well-known scientific phenomenon. When a dark surface is exposed to sunlight, it absorbs solar energy and becomes heated. Solar energy collectors operating on this principle typically consist of a surface oriented toward the sun, which absorbs a portion of the solar energy and transfers it to a working fluid in direct contact.

The basic thermal conversion devices, known as flat-plate collectors, are readily available and can function efficiently over a temperature range of up to approximately 365 K. These collectors are primarily used for tasks such as providing hot water and space heating, and in some cases, they can also support absorption-type air conditioning systems. Utilizing solar radiation for generating

low-temperature heat, like for hot water and swimming pool heating, is currently both technically feasible and economically practical.

In certain regions of the world, low-temperature thermal utilization is also employed for heating and cooling buildings. However, when higher working temperatures are required, such as for operating traditional steam engines, focusing devices in conjunction with absorber-receivers are necessary. These advanced systems have been able to achieve operating temperatures as high as 4000 K and have been effectively used to generate steam for powering irrigation pumps.

Presently, various concentrating devices for producing steam to generate electric power are under construction in different parts of the world. Cost estimates suggest that once these projects are completed, the cost of solar power in favorable locations will be competitive with that of conventional thermal power sources [9].

1.2.2 Concentrating Solar Energy

Concentrating Solar Power (CSP) has the potential to make a significant contribution to the world's energy supply. Given the urgent necessity to accelerate the development of advanced energy technologies to address global challenges such as clean energy, climate change, and sustainable development, the current decade presents a crucial window of opportunity for CSP to emerge as a competitive source of electrical power, particularly in the sunniest regions of the world, capable of meeting peak and intermediate energy demands.

CSP harnesses renewable solar resources to generate electricity, all the while producing minimal levels of greenhouse gas emissions. Consequently, it holds great promise as a pivotal technology for mitigating the impacts of climate change. Furthermore, the flexibility inherent to CSP plants enhances energy security. Unlike solar photovoltaic (PV) technologies, CSP possesses the inherent capability to store thermal energy for brief periods, which can be later converted into electricity. When coupled with thermal storage capacity, CSP facilities can maintain electricity production even when clouds obscure the sun or after sunset. CSP plants can also be equipped with backup power sources using combustible fuels. These attributes empower CSP to deliver dependable electricity that can be dispatched to the grid as needed, including during the evening peak demand or even around the clock to fulfill base-load energy requirements. Collectively, these characteristics position CSP as a promising technology for regions seeking clean, flexible, and reliable power solutions [2].

1.2.3 Limitations of Solar Energy

The primary challenge in the engineering design of equipment for harnessing solar energy is the low flux density, which necessitates large collection surfaces for widespread utilization. Larger surfaces, however, lead to increased energy costs. On clear, sunny days when the sun is directly overhead, a theoretical 10 m^2 surface could provide energy at a 70% efficiency of collection and 30% conversion efficiency, yielding about 2 kW. In practice, several factors reduce this potential.

The solar energy reaching Earth consists of two components: direct solar radiation and diffuse energy from the sky. The amount of direct energy depends on factors such as cloud cover and the sun's position, being highest on clear days. Some solar radiation is scattered by clouds, but not all of it is absorbed.

Another practical limitation is that a significant portion of solar energy is received in remote areas and would require transmission to industrialized nations. The highest average energy levels on a horizontal plane are found in desert areas around latitudes $25°$N and $25°$S of the equator, gradually decreasing toward the equator and the poles. Clouds can substantially reduce global irradiance in equatorial regions. Despite this, industrialized regions, particularly Europe, have been leaders in solar power deployment over the past decade.

The third limitation of solar energy as a large-scale power and heat source is its intermittency. Solar energy exhibits regular daily and annual cycles due to the Earth's rotation and its orbit around the sun, and it is unavailable during adverse weather conditions. These daily and seasonal variations, compounded by weather-related fluctuations, necessitate energy storage or the use of supplementary fuels. [9]

1.3 Energy Storage

The widespread adoption of solar energy systems requires effective means of storing the collected and converted energy. This need becomes particularly critical in areas where grid-connected photovoltaic power capacity is growing rapidly. In distributed grid-connected solar electric power systems, energy storage plays a vital role in managing the mismatch between supply and demand. Various storage options are available, with some being economically viable today, while others require further research and cost reductions.

For applications like building heating and cooling, sensible heat storage in materials like water or rocks is a practical solution. Passive storage, known as "thermal mass," is an intelligent approach to integrate storage with buildings by incorporating materials like stone, bricks, or phase-change materials into building components.

In the case of electrical energy production systems, dedicated storage systems are necessary. One option is to use solar energy to produce hydrogen, storing the energy in either gaseous or liquid form. While there are no significant technical barriers to large-scale hydrogen production, storage, and utilization, the efficiency of hydrogen production is relatively low, leading to high costs for hydrogen storage and delivery systems at present.

High-temperature thermal energy storage is particularly suitable for concentrating solar thermal power, also known as CSP, and is already employed at a large scale commercially. Incorporating storage into a CSP plant increases the initial capital costs but, in fact, reduces the levelized cost of energy (LCOE) because it enables the CSP power block to be used for more hours, increasing overall efficiency and cost-effectiveness [15].

Chapter 2

Fundamentals of Solar Radiation

2.1 Basic of light

In the following discussion, we will explore the nature of the light coming from the solar radiation and the interaction with matter. Understanding this behavior is of paramount importance for the objectives of our study.

2.1.1 Properties of light

The light we encounter in our daily lives constitutes just a fraction of the sun's overall energy emissions reaching the Earth. Sunlight is a type of "electromagnetic radiation," and the visible light we perceive represents only a small segment of the complete electromagnetic spectrum (illustrated on the figure). The electromagnetic spectrum characterizes light as a wave with a specific wavelength. In the early 1800s, experiments by Young, Arago, and Fresnel revealed that light exhibited interference effects, indicating its wave-like nature. By the late 1860s, light was recognized as part of the electromagnetic spectrum. However, issues arose when wave-based equations couldn't explain experiments involving heated objects' spectral emissions in the late 1800s. Planck (1900) introduced the concept of energy quanta, while Einstein (1905) correctly defined these quantum energy elements, known as photons. Today, quantum mechanics explains light's dual nature - it can be a wave or particle, termed "wave-particle duality." [11]

2.1.2 Energy of photon

A photon is characterized by its wavelength, denoted as λ, or equivalently by its energy, denoted as E. There exists an inverse relationship between the energy of a photon (E) and the wavelength of light (λ), as described by the equation

$$E = \frac{h \cdot c}{\lambda} \tag{2.1}$$

where "h" represents Planck's constant and "c" is the speed of light. This inverse relationship signifies that light composed of high-energy photons, such as "blue" light, possesses a short wavelength, while light comprising low-energy photons, like "red" light, exhibits a longer wavelength.

When working with "particles" such as photons or electrons, the electron-volt (eV) is a commonly used unit of energy, as opposed to the joule (J). An electron-volt is the energy required to raise an electron by 1 volt, equating to a photon with an energy of $1eV = 1.602 * 10^{-19}J$. [11]

2.1.3 Photon Flux

Photon flux is defined as the number of photons per second per unit area

$$\phi = \frac{\textbf{number of photons}}{s^2} \tag{2.2}$$

It is a crucial parameter for assessing the generation of electrons. However, photon flux alone doesn't provide information about the energy or wavelength of the photons. To calculate the power density for photons at a specific wavelength, you need to know both the photon's wavelength or energy and the photon flux at that wavelength.

Power density is determined by multiplying the photon flux by the energy of a single photon. Since photon flux tells you how many photons hit a surface in a given time, multiplying by the energy of the photons within the flux yields the energy striking a surface per unit time, which is equivalent to power density. To express power density in units of W/m^2, the energy of the photons should be in joules. [11]

The equations, using SI units, is:

$$H = \frac{\phi \cdot h \cdot c}{\lambda} \tag{2.3}$$

2.1.4 Spectral Irradiance

Spectral irradiance, denoted as F and expressed as a function of photon wavelength (or energy), is a prevalent method for characterizing a light source. It provides the power density at a specific wavelength. The units of spectral irradiance are in W/m^2µm, with "W/m^2"representing the power density at the given wavelength λ (in µm).Therefore"m^{-2}" pertains to the surface area of the light emitter, while "µm^{-1}" corresponds to the wavelength under consideration. Spectral irradiance can be calculated from the photon flux by converting the photon flux at a specific wavelength into W/m^2. This calculation involves dividing the photon flux at that wavelength by the given wavelength, in SI units, as depicted in the following equation: [11]

$$F(\lambda) = \phi \cdot E\frac{1}{\Delta\lambda} \tag{2.4}$$

2.1.5 Radiant Power Density

The total power density emitted from a light source can be determined by integrating the spectral irradiance over all wavelengths or energies

$$H = \int_0^\infty F(\lambda)d\lambda \tag{2.5}$$

However, a closed form equation for the spectral irradiance for a light source often does not exist.Instead the measured spectral irradiance must be multiplied by a wavelength range over which it was measured, and then calculated over all wavelengths.

The following equation can be used to calculate the total power density emitted from a light source [11].

$$H = \sum_{i} F(\lambda)\Delta\lambda \tag{2.6}$$

2.1.6 Blackbody Radiation

Many commonly encountered light sources, including the sun and incandescent light bulbs, can be closely approximated as "blackbody" emitters. A blackbody absorbs all incident radiation on its surface and emits radiation based on its temperature. The name "blackbody" arises from the fact that if they do not emit radiation in the visible range, they appear black due to the complete absorption of all wavelengths.The total power density from a blackbody is determined by integrating the spectral irradiance over all wavelengths which gives:

$$H = \sigma T^4 \tag{2.7}$$

where σ is the Stefan-Boltzmann constant and T is the temperature of the blackbody in kelvin [11].

2.2 Solar Radiation

In this section, we will discuss the most prevalent light source, which is the sun. Applying the terminology introduced in the previous section, it's worth noting that the sun can be characterized as a blackbody with a temperature of approximately 6000 Kelvin (K).

2.2.1 The Sun

The sun is a hot, gaseous sphere with internal temperatures exceeding 20 million Kelvin, primarily generated by nuclear fusion reactions within its core, where hydrogen is converted into helium. Radiation from the intensely hot core is not visible since it is absorbed by a layer of hydrogen atoms closer to the sun's surface. Heat is transferred through this layer via convection.

The sun's visible surface, known as the photosphere, maintains a temperature of approximately 6000 Kelvin and closely behaves as a blackbody. In detailed balance calculations, for simplicity, the spectrum corresponding to 6000 K is commonly utilized. However, more precise estimates of 5762 $\pm$50 K and 5730 $\pm$ 90 K have been proposed to better match the sun's actual spectrum. For the sake of consistency, we will employ the approximation of 5800 K.

Using the Equation (2.7), gives an emitted power density of the Sun of $64x10^6$ W/m^2. The total power emitted by the sun can be calculated by multiplying the emitted power density by the sun's surface area. With the sun's radius at $695x10^6m$, it has a surface area of approximately $6.07x10^{18}$ square meters. Thus, the total power output of the sun is $64x10^7$ times $6.09x10^{18}m^2$, resulting in $3.9x10^{26}$ Watts. This is an incredibly vast amount of power, especially when considering that the entire energy consumption of the world is only $\sim$ 18 terawatts ($18x10^{12}$ Watts) [11].

2.2.2 Solar Radiation in Space

Indeed, as an object in space moves further away from the sun, only a fraction of the total power emitted by the sun impinges upon it. This phenomenon is described by solar irradiance (H_0), which represents the power density received by an object due to the sun's illumination. At the sun's surface, the power density corresponds to that of a blackbody at approximately 6000K, and the total power output of the sun is obtained by multiplying this value by the sun's surface area.

However, as an object in space relocates farther from the sun, the total power from the sun is distributed over a significantly larger surface area. Consequently, the solar irradiance on the object decreases with increasing distance from the sun. This decrease in solar irradiance is a fundamental concept in understanding the diminishing intensity of sunlight as one moves away from the sun.

The solar irradiance (H_0) on an object situated at a distance (D) from the sun can be determined by dividing the total power emitted by the sun by the surface area over which the sunlight is distributed. The total solar radiation emitted by the sun can be expressed as Equation (2.7) multiplied by the surface area of the sun ($4\pi R_{sun}^2$), where R_{sun} is the radius of the sun.

The surface area over which the power from the sun is distributed will be $4\pi D^2$, where D is the distance of the object from the sun. Therefore, the solar radiation intensity (H_0) in (W/m^2), incident on an object, is calculated as follows:

$$H_0 = \frac{R_{\mathbf{sun}}^2}{D^2} H_{\mathbf{sun}} \tag{2.8}$$

This equation describes the solar irradiance on an object at distance D from the sun based on the sun's temperature (T), radius (R_{sun}), and the distance of the object from the sun (D).

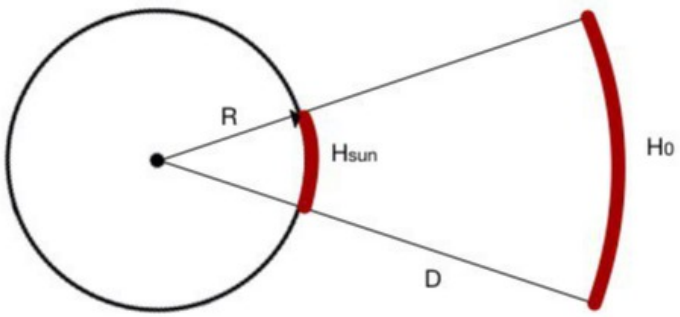

Figure 2.1: Solar Irradiance on a object at distance

Indeed, as an object moves further away from the sun, the same amount of solar power is distributed over a significantly larger surface area. This dispersion results in a reduction of the solar radiation power intensity at the location of the object. The distance between each planet and the Sun varies due to the elliptical shape of their orbits. The Earth-Sun distance, often referred to an astronomical unit (AU), is defined by the International Astronomical Union (IAU) as

approximately $149.59x10^9m$, making it a fundamental unit of measurement for distances within our solar system. [11]

2.2.3 Solar Radiation to Earth

Solar radiation outside Earth's atmosphere is computed using the solar power density (H_{sun}) at the sun's surface (approximately $6x10^7W/m^2$), the radius of the sun (R_{sun}), and the Earth-Sun distance. This calculation yields a solar irradiance of approximately $1.36kW/m^2$ at the Earth's atmosphere. About 60% of this amount reaches the surface of the earth, the rest is involved in the atmospheric behaviour.

Atmospheric effects have several significant impacts on solar radiation at the Earth's surface, particularly for solar applications:

- A reduction in the power of solar radiation due to absorption, scattering, and reflection within the atmosphere;
- A shift in the spectral composition of solar radiation due to greater absorption or scattering of specific wavelengths;
- The introduction of a diffuse or indirect component into the solar radiation, which affects its directionality;
- Local atmospheric variations, such as water vapor, clouds, and pollution, further influence the incident power, spectrum, and directionality of solar radiation. [11]

2.2.4 Solar Radiation on a Tilted Surface

The solar radiation received by a horizontal surface at ground level is the sum of three components: direct radiation (beam radiation), which directly impacts the surface; diffuse radiation, which encompasses the irradiance absorbed by molecules in the atmosphere and emitted in various directions, and reflected radiation, also known as albedo, which is the portion of radiation that is reflected by the ground and other objects.

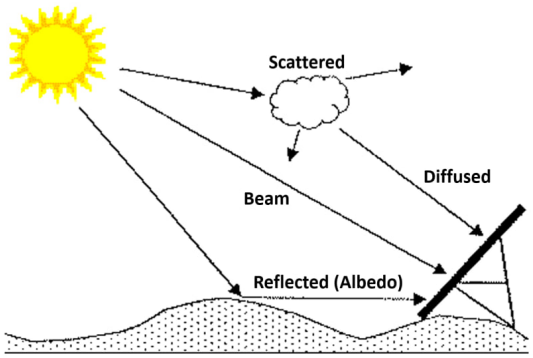

Figure 2.2: Attenuation of solar radiation

The solar radiation on an inclined surface with a tilt angle (β) from the horizontal and an azimuth angle (a_w), assumed to be west of south, as depicted in Figure 2.3, is the combination of

three components: direct beam radiation ($I_{\mathbf{b,c}}$), diffuse sky radiation ($I_{\mathbf{d,c}}$), and solar radiation reflected from the ground ($I_{\mathbf{r,c}}$).

$$I_{\mathbf{t}} = I_{\mathbf{b}} + I_{\mathbf{d}} + I_{\mathbf{r}} \tag{2.9}$$

If "i" represents the angle of incidence of beam radiation on the tilted surface, it can be straightforwardly demonstrated that the immediate beam radiation incident on the surface per unit area is

$$I_{\mathbf{b,c}} = I_{\mathbf{b,n}} \cdot \cos i \tag{2.10}$$

To find the diffuse radiation on the surface ($I_{\mathbf{d,c}}$), you can calculate it by multiplying the diffuse sky radiation on a horizontal surface by the view factor between the sky and the surface:

$$I_{\mathbf{d,c}} = I_{\mathbf{d,h}} \cdot F_{\mathbf{s,c}} \tag{2.11}$$

The ground-reflected solar radiation can be determined by taking into account the total solar radiation received by a horizontal surface and the ground reflectance (ρ), and it can be expressed as follows:

$$I_{\mathbf{r,c}} = \rho \cdot I_{\mathbf{h}} \tag{2.12}$$

With solar radiation on a horizontal surface given by

$$I_{\mathbf{h}} = (I_{\mathbf{b,n}} \cdot \sin \alpha + I_{\mathbf{d,h}}) \tag{2.13}$$

The portion of Ir intercepted by the inclined surface can be calculated by multiplying the ground-reflected radiation by the view factor between the surface and the ground, and this can be expressed as follows:

$$I_{\mathbf{r,c}} = \rho \cdot I_{\mathbf{h}} \frac{1 - \cos \beta}{2} = \rho \cdot I_{\mathbf{h}} (1 - F_{\mathbf{s,c}}) \tag{2.14}$$

For ordinary ground or grass, ρ is approximately 0.2, and for snow-covered ground, it can be taken as approximately 0.8. [9]

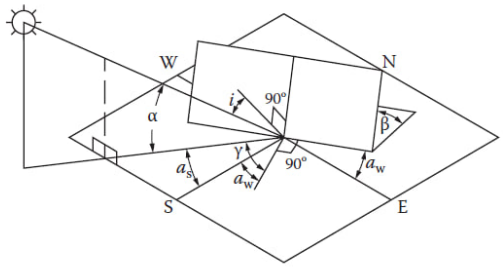

Figure 2.3: Definition of solar angles for tilted surface

2.3 Measuring the Solar Radiation

There are two primary types of instruments employed to measure solar radiation: pyranometers and pyrheliometers. A pyranometer possesses a hemispherical view of its surroundings, making it suitable for measuring total, direct, and diffuse solar radiation on a surface. Conversely, a pyrheliometer has a limited field of view, typically around 5 degrees, and is frequently utilized for measuring direct or beam solar radiation by aligning it with the sun's position. In some cases, pyranometers can also gauge sky diffuse radiation by employing a shadow band to obstruct direct sunlight.

A pyranometer comprises a flat sensor or detector with an unobstructed hemispherical field of view, allowing it to convert and correlate the total incident radiation on the sensor into a measurable signal. Pyranometers that use thermal detectors for measurements can experience significant errors when tilted away from the horizontal due to free convection. To mitigate these errors, the detector is enclosed within double hemispherical glass domes with high transmission properties. The second dome serves to minimize errors stemming from infrared radiative exchange between the sensor and the sky. Typically, a desiccator is included to prevent condensation effects on the sensor or the dome. To measure sky diffuse radiation, a shade ring can be attached to the pyranometer, as illustrated in Figure 2.28, to block direct beam radiation throughout the day. The position of the shade ring is periodically adjusted in response to changes in solar declination.

Beam or direct solar radiation is generally quantified using a device known as a pyrheliometer. Essentially, a pyrheliometer positions the detector at the base of an elongated tube. This design restricts the detector's sky view to a narrow-angle of about 5°. When the tube is oriented toward the sun, the detector measures the beam solar radiation along with a small portion of the diffuse solar radiation within its viewing angle [29].

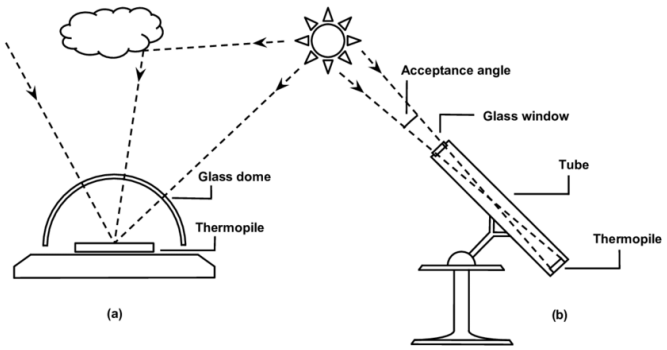

Figure 2.4: Schematic illustration of a pyranometer(a) and a pyrheliometer (b) [29]

2.3.1 Detectors for Solar Radiation Instrumentation

Solar radiation detectors come in four basic types: thermomechanical, calorimetric, thermoelectric, and photoelectric. Among these, thermoelectric and photoelectric detectors are the most commonly used today.

Thermoelectric detectors utilize a thermopile, which is composed of a series of thermocouple junctions. The thermopile generates a voltage that is directly proportional to the temperature

difference between the hot and cold junctions, which, in turn, is proportional to the incident solar radiation.

Photovoltaic detectors typically employ silicon solar cells to measure the short circuit current. These detectors are advantageous because they have a simple construction and do not require clear domes or convection-suppressing devices since heat transfer is not a concern. They are also insensitive to tilting, as natural convection does not affect their output. However, a key limitation of photovoltaic detectors is their spectral selectivity. They cannot measure radiation with wavelengths longer than the band gap of the photovoltaic detector, and silicon's band gap is 1.07 eV, equivalent to a wavelength of 1.1 μm. As a result, photovoltaic detectors are insensitive to changes in the infrared part of solar radiation, which includes wavelengths greater than $1.1\mu m$ [11].

2.3.2 Solar Radiation Data

Solar radiation data have been measured and recorded at various locations worldwide. Additionally, data for numerous other locations have been estimated using measurements taken at comparable climatic sites. [9]

Chapter 3

Solar Thermal Collectors

Converting the sun's radiant energy into heat has a long history and has evolved into a well-established solar conversion technology. The fundamental principle of solar thermal collection is that when solar radiation reaches a surface, a portion of it is absorbed, leading to an increase in the surface's temperature. The efficiency of a surface as a solar collector relies on not only its ability to absorb solar energy but also its capacity to minimize thermal and reradiation losses to the surroundings, as well as its effectiveness in extracting and utilizing the collected energy. This chapter analyzes in detail the family of Concentrated Solar Collectors due to they were used for this study.

To capture the solar radiation discussed in Section 2.1, Concentrating Solar Power (CSP) plants employ mirrors to focus sunlight onto a receiver, which captures and channels the solar energy to a heat transfer fluid. This thermal energy can be used to supply heat for various applications or to generate electricity through traditional steam turbines. In the case of large CSP plants, they can include a heat storage system, enabling them to provide heat or generate electricity during periods without direct sunlight, such as at night or under cloudy skies.

CSP facilities rely on abundant direct solar irradiance to function effectively, making them particularly suitable for deployment in the Sun Belt region, which encompasses areas between 40 degrees north and south of the equator. This region encompasses regions such as the Middle East, North Africa, South Africa, India, the southwestern United States, Mexico, Peru, Chile, western China, Australia, southern Europe, and Turkey. In most of these regions, the technical potential for CSP-based electricity generation significantly exceeds their electricity demand, offering opportunities for electricity export through high-voltage transmission lines.

One of CSP's key advantages over photovoltaic solar systems (PV) lies in its ability to integrate cost-effective thermal energy storage, allowing for the provision of intermediate- and base-load electricity. This capability substantially raises the capacity factor of CSP plants and enhances the dispatchability of the electricity they generate, thereby improving grid integration and the economic competitiveness of such power plants.

In contrast to solar photovoltaics (PV), which capture a broad spectrum of sunlight, CSP exclusively utilizes the direct component of sunlight (DNI). Therefore, CSP can provide carbon-free heat and power efficiently in regions characterized by high DNI, typically found in Sun Belt regions. [14]

3.1 Radiative Properties and Characteristics of Materials

When radiation strikes an object, a portion of it is reflected, another portion is absorbed, and, if the material is transparent, a portion is transmitted, as illustrated in Figure 3.1.

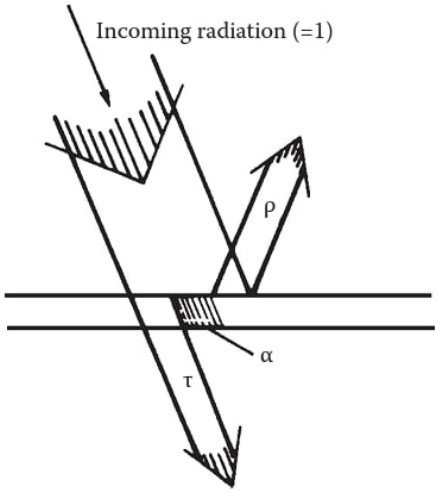

Figure 3.1: Ligt diffraction

The fraction of incident radiation that is reflected is referred to as reflectance (ρ), the fraction that is absorbed is absorptance (α), and the fraction that is transmitted is transmittance (τ). According to the first law of thermodynamics, the sum of these three components must be equal to one, or

$$\alpha + \tau + \rho = 1 \tag{3.1}$$

For opaque objects, which do not transmit any radiation, τ is equal to zero.

The reflection of radiation can be categorized as either specular or diffuse. Specular reflection occurs when the angle of incidence equals the angle of reflection, resulting in a well-defined reflection direction. In contrast, diffuse reflection involves the scattering of reflected radiation in various directions, lacking a specific reflection angle. In practice, no surface is purely specular or diffuse, but a highly polished surface tends to exhibit specular reflection, while a rough surface scatters radiation diffusely.

Another important radiative property is emittance (ϵ), which is the ratio of the radiative emissive power of a real surface to that of an ideal "black" surface, as defined in 2.1.6. All of these radiative properties, α, τ, ρ, and ϵ, can be influenced by the wavelength and direction of the incident radiation [14].

3.1.1 Selective Surface

Selective absorber surfaces are crucial components in solar collector systems due to their unique ability to efficiently capture solar radiation while minimizing heat loss. These surfaces achieve this by having high absorptance for short-wavelength solar radiation and low emittance for the typical operating temperature of the surface.

This combination of surface characteristics is achievable because a significant portion of the energy in incoming solar radiation, approximately 98%, falls within wavelengths below 3 μm. In contrast, when we consider black or gray surfaces operating at temperatures around 400 K, about 99% of the radiation they emit occurs at longer wavelengths exceeding 3 μm. This difference in spectral distribution allows selective absorber surfaces to capture solar energy effectively while reducing heat loss through radiation.

The performance of selective absorber coatings deteriorates as temperatures rise to $400°$C and beyond. With the growing interest in concentrated solar thermal power and the construction of power plants as large as 300 megawatts electric (MWe), there is a pressing requirement for selective solar absorbers that can sustain optimal performance even at temperatures exceeding $400°$C [14].

3.1.2 Reflecting Surface

Concentrating solar collectors necessitate the use of either highly specular reflecting surfaces in the solar spectrum or transparent refractive devices with high transmittance in the solar spectrum. Reflecting surfaces are typically achieved using highly polished metals or metal coatings applied to suitable substrates. When opaque substrates are employed, the reflective coatings are usually placed on the front surface, such as chrome plating on copper or polished aluminum.

However, when a transparent substrate is used, the reflective coating can be applied to either the front or back surface. In the case of a back-surfaced reflector, solar radiation must pass through the substrate twice, making the transmittance of the material a critical factor to consider.

3.2 Concentrating Solar Collector

Concentration of solar radiation involves directing the solar flux incident on an aperture area ($A_{\mathbf{a}}$) onto a smaller receiver or absorber area ($A_{\mathbf{r}}$). There are two primary ways to express this concentration: the optical concentration ratio ($C_{\mathbf{R,o}}$) and the geometric concentration ratio ($C_{\mathbf{R}}$).

The optical concentration ratio ($C_{\mathbf{R,o}}$) is defined as the ratio of the solar flux ($I_{\mathbf{r}}$) received by the absorber to the flux ($I_{\mathbf{a}}$) incident on the aperture. Mathematically, it is represented as

$$C_{\mathbf{R,o}} = \frac{I_{\mathbf{r}}}{I_{\mathbf{a}}} \tag{3.2}$$

$C_{\mathbf{R,o}}$ provides a genuine measure of concentration as it considers the optical losses that occur due to the reflecting and refracting components. However, it doesn't provide insights into the thermal losses, which are influenced by the size of the receiver area.

The geometric concentration ratio ($C_{\mathbf{R}}$), on the other hand, is based on the comparison of the two areas (A_a and A_r). It is calculated as

$$C_{\mathbf{R}} = \frac{A_{\mathbf{a}}}{A_{\mathbf{r}}} \tag{3.3}$$

While $C_{\mathbf{R,o}}$ focuses on the optical aspect, $C_{\mathbf{R}}$ takes into account the relationship between the two areas but doesn't consider optical losses.

Concentrating solar collectors inherently offer higher efficiency at a given temperature when compared to flat-plate collectors. This advantage arises from the fact that the area from which

heat is lost in concentrators is smaller than the aperture area. In a flat-plate collector, both these areas are of equal size. To illustrate this concept, we can use a simple energy balance equation:

The useful energy delivered by a collector, $q_{\mathbf{u}}$, is given by:

$$q_{\mathbf{u}} = \eta_{\mathbf{o}} \cdot I_{\mathbf{c}} \cdot A_{\mathbf{a}} - U_{\mathbf{c}}(T_{\mathbf{r}} - T_{\mathbf{a}})A_{\mathbf{r}} \tag{3.4}$$

Where $\eta_{\mathbf{o}}$ is the optical efficiency, $I_{\mathbf{c}}$ is the solar radiation incident on the collector, $U_{\mathbf{c}}$ is the overall heat loss coefficient, $T_{\mathbf{r}}$ is the collector temperature and $T_{\mathbf{a}}$ is the ambient temperature.

The instantaneous collector efficiency is represented as η_c, and it's given by:

$$\eta_{\mathbf{c}} = \frac{q_{\mathbf{u}}}{I_{\mathbf{c}} \cdot A_{\mathbf{a}}} \tag{3.5}$$

by rearranging and using Equation (3.4), we arrive at:

$$\eta_{\mathbf{c}} = \eta_{\mathbf{o}} - \frac{U_{\mathbf{c}}(T_{\mathbf{r}} - T_{\mathbf{a}})}{I_{\mathbf{c}}} \frac{1}{C_{\mathbf{R}}} \tag{3.6}$$

For flat-plate collectors, $C_{\mathbf{R}}$ is approximately equal to 1, whereas for concentrators, $C_{\mathbf{R}}$ is greater than 1. Consequently, the loss term (the second term) in Equation (3.6) is smaller for concentrators, leading to higher efficiency. However, it's important to note that this analysis is a simplification and doesn't account for the reduction in optical efficiency that can occur due to imperfect mirrors or lenses used in concentrators.

The evaluation of $U_{\mathbf{c}}$ in Equation (3.6) is challenging for high-temperature concentrators, mainly due to the significant impact of radiation heat loss, which introduces non-linearities proportional to T^4.

One drawback of concentrators is their limited ability to collect a small fraction of the diffuse energy incident on their aperture. This limitation plays a crucial role in determining the geographic suitability of concentrators for specific applications [14].

3.2.1 Concentrator Types

Concentrating Solar Power (CSP) technology comprises four primary variants: Parabolic Trough (PT), Fresnel Reflector (FR), Solar Tower (ST), and Solar Dish (SD). PT and FR plants concentrate sunlight onto a focal line and typically achieve maximum operating temperatures ranging from $300°C$ to $550°C$. In contrast, ST and SD plants concentrate sunlight onto a single focal point and have the capacity to reach even higher temperature [27].

Parabolic Trough (PT)

Parabolic Trough (PT) technology represents the most established segment within Concentrating Solar Power (CSP), contributing to over 90% of the current installed CSP capacity. PT systems rely on parabolic mirrors designed to concentrate the sun's rays onto heat receivers, typically steel tubes positioned along the focal line. These receivers are equipped with specialized coatings to maximize energy absorption and minimize infrared re-irradiation, and they operate within evacuated glass enclosures to prevent convection heat losses.

The collected solar heat is transferred via a heat transfer fluid (e.g., synthetic oil or molten salt) flowing within the receiver tube and then conveyed to a steam generator. This process

generates superheated steam, which, in turn, drives the turbine. Both the mirrors and receivers are designed to track the sun's movement along a single axis, usually from East to West.

A tracking system needs to be dependable and capable of accurately following the sun, resetting the collector to its initial orientation at the day's end or during nighttime. It should also adapt to changes caused by intermittent cloud cover. Furthermore, tracking mechanisms serve to safeguard collectors by shifting them out of focus, shielding them from adverse environmental factors and operational challenges, such as strong winds, overheating, or issues with the thermal fluid flow system.

The level of precision required in the tracking mechanism hinges on the collector's acceptance angle [27].

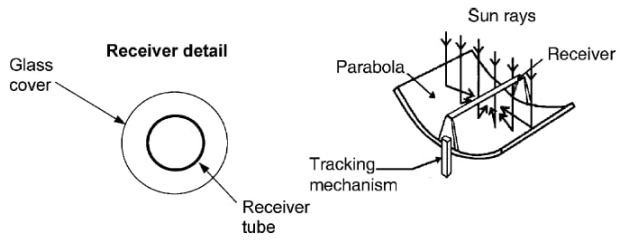

Figure 3.2: Schematic of a parabolic trough collector [27]

Most operational PT plants currently have capacities ranging from 14 to 80 Megawatts electric (MWe), with efficiencies averaging around 14-16% (i.e., the ratio of solar irradiance power to net electric output) and maximum operating temperatures of $390°C$. This temperature limit is mainly due to the degradation of synthetic oil used for heat transfer. Ongoing demonstrations involve the use of high-temperature molten salt at $550°C$ for either heat transfer or storage, with the potential to enhance plant efficiency (e.g., to 15%-17%) and increase thermal storage capacity [27].

Fresnel Reflector (FR)

Fresnel Reflector (FR) plants share similarities with PT plants but employ a configuration of ground-based, flat or slightly curved mirrors, positioned at varying angles to focus sunlight onto a stationary receiver situated several meters above the mirror field. Each row of mirrors incorporates a single-axis tracking system to concentrate sunlight onto the fixed receiver.

In Figure 3.3, you can see an illustration of an element within an LFR (Linear Fresnel Reflector) collector field. The most significant advantage of this system is its use of flat or elastically curved reflectors, which are more cost-effective when contrasted with parabolic glass reflectors. Moreover, these reflectors are positioned near the ground, resulting in reduced structural demands.

The receiver comprises an elongated, selectively-coated tube where flowing water is transformed into saturated steam through a process known as Direct Steam Generation (DSG). Due to potential astigmatism-induced distortions in the focal line of the FR plant, a secondary mirror is placed above the receiver to redirect and refocus the sun's rays. While the optical efficiency of the FR system may be lower than that of PT systems, leading to higher optical losses, the relative simplicity of the FR plant translates to reduced manufacturing and installation costs when

compared to PT plants [27].

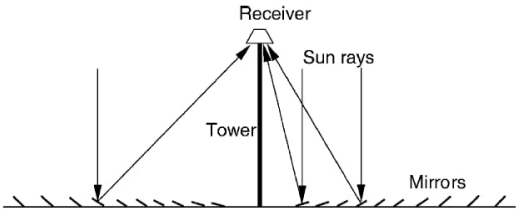

Figure 3.3: Schematic diagram of a downward facing receiver illuminated from an LFR field [27]

Solar Tower (ST)

In Solar Tower (ST) plants, a multitude of computer-assisted mirrors, also known as heliostats, individually track the sun across two axes. They concentrate solar irradiation onto a single receiver positioned atop a central tower, where the solar heat drives a thermodynamic cycle that generates electricity.

Collector and receiver systems can be categorized into three general configurations. In the first configuration, heliostats encircle the receiver tower, and the receiver, typically cylindrical, features an external heat transfer surface. In the second configuration, heliostats are positioned north of the receiver tower (in the northern hemisphere), and the receiver incorporates an enclosed heat transfer surface. In the third configuration, the heliostats are also located north of the receiver tower, and the receiver, which is oriented as a vertical plane, possesses a heat transfer surface facing north.

ST plants, in principle, have the capacity to achieve higher temperatures compared to PT and FR systems, thanks to their higher concentration factors. These plants can employ various primary heat transfer fluids, including water-steam (Direct Steam Generation or DSG), synthetic oil, molten salt, and there's even consideration of using high-temperature gases.

DSG in the receiver eliminates the need for a heat exchanger between the primary heat transfer fluid (e.g., molten salt) and the steam cycle but presents challenges for thermal storage. Depending on the primary heat transfer fluid and the receiver's design, maximum operating temperatures may span from 250-300$^{\circ}C$ (utilizing water-steam) to 390$^{\circ}C$ (with synthetic oil) and up to 565$^{\circ}C$ (using molten salt). Temperatures exceeding 800$^{\circ}C$ can be attained when high-temperature gases are employed.

The temperature level of the primary heat transfer fluid determines the operating conditions (subcritical, supercritical, or ultra-supercritical) of the steam cycle in the conventional part of the power plant.

High-temperature Solar Tower (ST) plants present the prospect of significant advantages when compared to other Concentrating Solar Power (CSP) technologies. These potential benefits encompass enhanced efficiency, improved heat storage capabilities, superior performance, higher capacity factors, and potentially reduced costs. In the long term, they may emerge as the most cost-effective source of CSP-generated electricity.

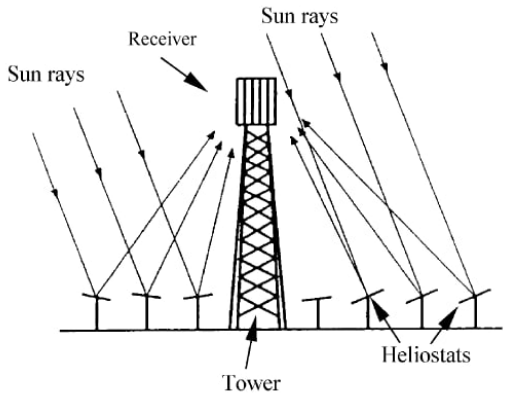

Figure 3.4: Schematic of a Central Receiver System [27]

Solar Dishes (SD)

A parabolic dish reflector, as depicted in Figure 3.5, serves as a point-focus collector that continuously tracks the sun in two axes. Its primary function is to concentrate solar energy onto a receiver positioned at the dish's focal point. The dish's orientation must accurately follow the sun's movement to ensure that the concentrated solar beam is directed into the thermal receiver.

Within the receiver, the radiant solar energy is absorbed and transformed into thermal energy through a circulating fluid. This thermal energy can be further utilized in two main ways: it can be converted into electricity by connecting an engine-generator directly to the receiver, or it can be transported via piping to a central power-conversion system for broader applications.

Notably, parabolic dish systems have the capability to achieve extremely high temperatures, surpassing $1500°C$. Since the receivers are dispersed across the collector field, similar to how parabolic troughs are arranged, parabolic dishes are often referred to as distributed receiver systems. [27]

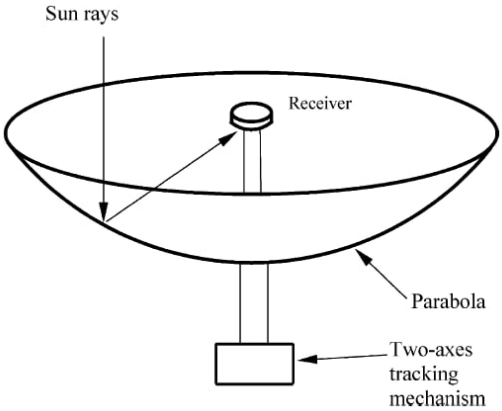

Figure 3.5: Schematic of a parabolic dish collector [27]

3.2.2 Optycal Analisys

The concentration ratio (C) is a measure defined as the ratio of the aperture area to the receiver or absorber area Equation (3.3). In the case of Flat Plate Collectors (FPC) with no reflectors, the concentration ratio is 1. However, for concentrators, which are designed to focus sunlight onto a receiver, the concentration ratio is always greater than 1.

For a single-axis tracking collector, the maximum achievable concentration is determined by the formula

$$C_{\mathbf{max}} = \frac{1}{\sin \theta_{\mathbf{m}}} \tag{3.7}$$

where $\theta_{\mathbf{m}}$ represents the half acceptance angle. The half acceptance angle indicates the coverage of half of the angular zone in which the concentrator's receiver can capture radiation effectively. Radiation is collected over an angle of $2\theta_{\mathbf{m}}$ because sunlight incident within this angle passes through the aperture and reaches the receiver. This angle defines the angular field within which radiation can be collected by the receiver without the need for continuous tracking of the concentrator.

The incidence angle for different tracking modes, whether single-axis or dual-axis, is a crucial factor to consider. In the case of single-axis tracking, the motion can occur in various directions, such as east-west, north-south, or parallel to the Earth's axis. The choice of tracking mode significantly impacts the amount of incident radiation that falls onto the collector surface, and this incident radiation is typically proportional to the cosine of the incidence angle.

The following table (Figure 3.6) illustrates the amount of energy received on a $1m^2$ surface for four tracking modes during the summer and winter solstices and the equinoxes. The performance of these tracking modes is compared to the full tracking mode, which is capable of collecting the maximum amount of solar radiation and is represented as 100% in the comparison. This comparison helps evaluate how effectively different tracking modes capture solar energy in various seasonal conditions.

Tracking mode	Solar energy (kW h/m^2)			Percent to full tracking		
	E	SS	WS	E	SS	WS
Full tracking	8.43	10.60	5.70	100.0	100.0	100.0
E–W polar	8.43	9.73	5.23	100.0	91.7	91.7
N–S horizontal	6.22	7.85	4.91	73.8	74.0	86.2
E–W horizontal	7.51	10.36	4.47	89.1	97.7	60.9

Note: E: equinoxes, SS: summer solstice, WS: winter solstice.

Figure 3.6: Comparison of energy absorbed for various modes of tracking

Therefore, optical efficiency, in the context of solar collectors, is a measure defined as the ratio of the energy absorbed by the receiver to the energy incident on the collector's aperture. This optical efficiency is influenced by several factors, including the optical properties of the materials used, the collector's geometry, and imperfections that can arise during the collector's construction.

Mathematically, optical efficiency can be expressed by the equation:

$$\eta_{\mathbf{o}} = \rho \cdot \pi \cdot \alpha \cdot \gamma[(1 - A_{\mathbf{f}} \cdot \tan(\theta)\cos(\theta)] \tag{3.8}$$

The geometry of the collector plays a significant role in determining the geometric factor, denoted as "$A_{\mathbf{f}}$." This factor quantifies the effective reduction of the aperture area due to the influence of abnormal incidence effects. In essence, $A_{\mathbf{f}}$ accounts for how the collector's design and shape impact the amount of sunlight that can be effectively captured and converted into usable energy by the receiver [27].

Chapter 4

Storage systems

In conventional power plants, the stored fuel within the plant serves as both the energy source and the energy storage system. Additional energy storage is typically not required in these setups.

However, in the case of solar thermal power plants, integrating an energy storage system offers several notable advantages. These advantages include:

- Higher Annual Solar Contribution: Energy storage enables a solar thermal power plant to consistently provide a higher annual contribution of solar energy. This is especially valuable in areas where solar irradiation varies due to factors like day-night cycles, seasonal changes, daily fluctuations, and weather conditions;

- Reduction of Part-Load Operation: Energy storage helps minimize part-load operation of the power plant, thereby enhancing overall efficiency and operational flexibility. This is achieved by utilizing stored energy during periods of reduced sunlight;

- Effective Power Management: Energy storage systems facilitate improved power management by storing surplus energy when solar irradiation is abundant and releasing it during periods of high demand or when solar input is limited;

- Buffer Storage: Energy storage acts as a buffer to compensate for the intermittent and varying nature of solar irradiation throughout the day and under different weather conditions.

By incorporating energy storage, solar thermal power plants enhance the reliability and security of their energy supply. In some solar thermal power plants equipped with energy storage systems, operations can continue for many hours after sunset, ensuring a more consistent power supply. In contrast, a solar thermal power plant without an energy storage system can only operate between sunrise and sunset, unless it is combined with other energy sources or storage solutions.

When properly designed with a suitably sized thermal energy storage system and a backup system using fossil fuels, Concentrated Solar Power (CSP) technologies offer a dependable capacity to generate power on demand. This sets them apart from other renewable technologies such as Photovoltaic (PV) and wind power, which can only provide variable and fluctuating power outputs.

As the share of power generated by renewable energies is targeted to exceed approximately

35% of total power generation, CSP becomes a critical component. This is because, as a dispatchable renewable power technology, CSP can effectively fill the gaps created by the intermittent nature of PV and wind power. By utilizing thermal energy storage and a fossil backup system, CSP plants can operate as baseload power plants. This is advantageous and, for instance, is crucial for applications like seawater desalination, where a continuous and steady power supply is essential.

However, in the absence of thermal energy storage and a fossil backup system, CSP does not have a clear advantage over PV. This is because CSP technologies tend to be more complex than PV and lack the modular extendability that PV offers.

This chapter explores various types of thermal energy storage systems that have been employed in existing solar thermal power plants, shedding light on the importance of these systems in maximizing the effectiveness of CSP technologies in the context of a growing renewable energy landscape. [10]

4.1 Thermal Energy Storage Types

The subsequent section provides a description of various thermal energy storage options for use in solar thermal power plants. These thermal energy storage types can be broadly categorized into four main groups:

1. Thermal Energy Storage System for sensible Heat
    - Indirect Storage Systems
    - Direct Storage Systems
2. Latent Heat Storage
3. Steam Accumulator
4. Thermo-Chemical Storage System

Each of these four groups will be elaborated upon in the following pages. [10]

4.1.1 Thermal Energy Storage for sensible Heat

The concept of sensible heat pertains to the heat that is either absorbed or released by a material due to a change in temperature, without the material undergoing any change in its aggregate state. The energy capacity of the storage material, measured in joules (J) or kilowatt-hours (kWh), is determined by the temperature difference, in conjunction with the material's thermophysical properties such as density, specific heat, and its volume:

$$E_{\mathbf{s}} = \rho \cdot V \int_{T_{\mathbf{c}}}^{T_{\mathbf{h}}} c_p(T) dT \tag{4.1}$$

Favorable characteristics of sensible heat storage materials encompass high densities (ρ) in kilograms per cubic meter (kg/m^3), substantial specific heat capacities (c_p) in joules per kilogram per Kelvin (J/kg-K), and significant temperature differentials between the hot and cold states ($T_{\mathbf{h}}$ - $T_{\mathbf{c}}$) in Kelvin (K). Thermal energy storage systems for sensible heat can be categorized into

two main types: indirect storage and direct storage. [15] Presently, the practical application of high-temperature sensible heat storage for electricity generation involves the utilization of both liquids, such as molten salts, and solid materials like concrete and rocks. [10]

Indirect Storage Systems

In a indirect sensible heat storage systems, heat is stored in a material separate from the primary heat transfer fluid. Heat is transferred from a primary heat transfer fluid to the storage material and subsequently released when needed. This approach allows for greater design flexibility because the storage material can be optimized for storage performance, while the primary heat transfer fluid can be chosen based on process requirements. Indirect sensible heat storage systems often employ a secondary heat transfer fluid to facilitate heat transfer between the primary heat transfer fluid and the storage material. [10]

Direct Storage Systems

In a direct sensible heat storage system, the heat storage material is directly exposed to the heat source. This means that the heat transfer fluid circulates through the heat storage material and directly exchanges heat with it. Direct sensible heat storage systems often consist of tanks or coils heated by a heat source, such as the heat transfer fluid directly heated by solar collectors. This type of storage is effective for rapidly storing and releasing heat, but it may require specific materials and design considerations to ensure proper thermal insulation. [10]

Liquid

Molten nitrate salt, typically consisting of 60% sodium nitrate (N_aNO_3) and 40% potassium nitrate (KNO_3), is widely employed in commercial Concentrated Solar Power (CSP) plants worldwide to offer substantial thermal energy storage capabilities, often in the gigawatt-hour range. This particular molten salt possesses a low vapor pressure, allowing it to operate without pressurization under typical storage temperatures of up to approximately $600°$C. Additionally, it can be efficiently pumped from one location to another. CSP plants are capable of achieving substantial capacity factors, typically in the range of 70-80%, and they offer dispatchable energy, making them an efficient and reliable source of renewable power. [10]

Solid

Solid thermal storage has found applications in various commercial and demonstration facilities. In 2011, Graphite Energy developed a 3-megawatt electric (MWe) Concentrated Solar Power (CSP) plant in Lake Cargelligo, New South Wales, Australia, which employed graphite blocks within receivers situated on multiple towers. These graphite blocks, when exposed to concentrated sunlight, served a dual role as the storage system and the boiler, generating steam for power production.

EnergyNest, a Norwegian company, designed a thermal energy storage system based on concrete. This system comprises an array of modular pipes filled with concrete and steel tubes. The tubes carry a heat-transfer fluid that can either heat the concrete during charging or extract heat from it during discharging to drive a turbine/generator or provide process heating. This system

offers the capability to charge and discharge in approximately 30 minutes, with stored energy lasting for several days and experiencing less than 2% heat loss per 24 hours in the case of large-scale systems. [10]

4.1.2 Latent-Heat Storage System

When it comes to storing latent heat, the process relies on the property of materials to absorb or release heat energy during a phase change. Consequently, latent-heat storage systems employ a phase change material (PCM) as the storage medium. In principle, there are three potential phase changes that can be utilized:

- solid-solid
- solid-liquid
- liquid-vapour

The utilization of a phase change from solid to solid is infrequent. In this case, the phase change occurs as the solid PCM changes its crystalline form. Similarly, the phase change from liquid to vapor is seldom used. In the present development of latent-heat storage systems, the phase change from solid to liquid plays a pivotal role, which will now be explored further.

During the charging process of the storage system, the solid PCM is melted, and during discharging, the fluid PCM becomes cooler and solidifies. The melting and solidification process can occur at either a constant melting temperature or within a specific temperature range, depending on the composition of the PCM. Maintaining constant process temperatures is generally preferable for the stable operation of a power plant.

In latent-heat storage systems designed for medium and high-temperature applications, materials are selected with melting temperatures that align with the operational temperature range. Depending on the mass or volume of the storage medium, it's possible to store significantly more energy using such a phase change material compared to materials like concrete.

For applications in medium or high-temperature ranges, certain phase change materials, especially nitrate and nitrite salts, are commonly considered. While some salts, such as hydroxides, have high melting enthalpies, they are often excluded due to their corrosive properties or elevated costs.

The total heat, denoted as Q (measured in joules), stored in a latent-heat storage system comprises three components:

- Q_{sol} (sensible heat): This term represents the energy required to heat the PCM from its solid state at a temperature of θ_{min} to the melting temperature, θ_{melt}.
- Q_{melt} (latent heat): This component corresponds to the energy needed to facilitate the melting of the PCM.
- Q_{liq} (sensible heat): This term accounts for the energy necessary to heat the liquid PCM to the desired storage temperature, θ_{max}.

The storage capacity, denoted as Q, of a latent-heat storage system can be calculated based on the temperature changes that the storage material undergoes during its operation. The formula for this calculation is as follows:

$$Q = m \cdot f_{\mathbf{u}}(c_{p,\mathbf{sol,m}}\Delta\theta_{\mathbf{min/melt}} + \Delta H_{\mathbf{melt}} + c_{p,\mathbf{liq,m}}\Delta Q_{\mathbf{melt/max}}) \tag{4.2}$$

Where:

- $f_{\mathbf{utilisation}}$ is the actual storage material utilisation coefficient,
- m is the mass of the storage material [kg]
- $c_{p,\mathbf{m}}$ is the mean heat capacity (note: subscript m stands for mean, sol for solid and liq for liquid) [J/(kgK)],
- $\Delta\theta_{\mathbf{min/melt}}$ is the temperature difference of the melting temperature and the minimum temperature of the phase change material in solid phase [K],
- $\Delta\theta_{\mathbf{melt/max}}$ is the temperature difference of the maximum temperature and the melting temperature of the phase change material in liquid phase [K], and
- $\Delta H_{\mathbf{melt}}$ is the specific melting enthalpy [J/kg].

This formula allows for the calculation of the energy storage capacity (Q) in joules (J). It considers various factors, including the mass of the storage material, its heat capacity, and the temperature differences associated with the phase change of the material. Due to the differing physical properties between the solid and liquid phases of the storage medium, the equation must account for two distinct specific heat capacities, denoted as $cp, solid$ for the average heat capacity of the solid phase and $cp, liquid$ for the average heat capacity of the liquid phase of the storage medium. [10]

4.1.3 Steam Accumulator

Steam accumulators are pressurized vessels where a charging system introduces steam into hot water, ensuring even distribution. This input of latent heat of condensation elevates the temperature of the hot water in the storage vessel. Steam accumulators leverage the most environmentally friendly and cost-effective heat transfer fluid (HTF) available. However, the necessary pressure vessels are a significant cost driver in terms of investment.

While categorized as a distinct type of thermal energy storage system, a steam accumulator can also be seen as a specialized form of direct storage system. It's important to distinguish between two scenarios: [10]

1. If the primary circuit's HTF is steam and a steam accumulator is employed, then steam is directly stored. In this situation, the steam accumulator can be considered a direct storage system.
2. Conversely, if the primary circuit's HTF is not steam, the steam accumulator can optionally be integrated into the steam cycle. However, this no longer aligns with the criteria of a direct storage system and, strictly speaking, does not fit the definition of an indirect storage system either.

4.1.4 Thermo-Chemical Energy Storage

Thermo-chemical energy storage systems utilize reversible reactions that store energy. These reactions are endothermic during the charging phase, absorbing energy, and exothermic during the discharging phase, releasing energy. The specific enthalpy of these reactions, which represents the heat content, is approximately one order of magnitude smaller than that of fossil fuel combustion but significantly larger than the storage of sensible or latent heat. It's worth noting that this technology is in its early stages of development. However, in the long term, it has the potential to offer cost-effective solutions and the promise of continuous, round-the-clock electricity generation.

In certain catalytic reactions, such as the back reaction, achieving reversibility necessitates the use of a catalyst rather than a simple change in the chemical balance. This allows the reaction products to be stored alongside each other without undergoing a reverse reaction. When the reacting substances and the catalyst form a homogeneous mixture, meaning they are either both gaseous or dissolved in a fluid, this is known as homogeneous catalysis. In heterogeneous catalysis (surface catalysis), the reacting substances are gaseous or dissolved in a fluid, while the catalyst exists in a solid form.

In the case of thermal dissociation, the initial substance AB exists in a solid or liquid state. By supplying the molar reaction enthalpy at temperature T_1 and a corresponding pressure p_1, the chemical bond between the substance pair AB is broken. The product A then exists in a solid or liquid state, while B becomes gaseous. This process is often referred to as heterogeneous evaporation. Reversing this process, known as absorption, occurs when the balance is disrupted through a reduction in temperature or an increase in pressure. In this process, B becomes the absorptive material, A acts as the absorbent, and AB is the absorbate. During this process, the reaction enthalpy released during the dissociation is utilized for energy storage. To store energy effectively, the products A and B must be stored separately. [10]

Chapter 5

Solar Thermal Power

In 1878, a compact solar power plant made its debut at the World's Fair in Paris. This solar installation harnessed sunlight by concentrating it through a parabolic reflector onto a steam boiler positioned at the reflector's focal point. The focused sunlight heated the water in the boiler, generating steam that powered a small reciprocating steam engine. This engine, in turn, operated a printing press. [9]

However, with the growing accessibility of affordable oil and natural gas, the enthusiasm for solar energy as a means of power production diminished. In this chapter, we will discuss the current state of power production through solar collectors.

5.1 Thermodynamic Power Cycles

There are two fundamental approaches to generating solar electric power. The first is through the photovoltaic process, which involves a direct conversion of energy. The second approach entails converting sunlight into heat at high temperatures and then using this thermal energy to drive a thermodynamic power cycle, ultimately converting the mechanical energy produced into electricity. This indirect approach is known as solar thermal power, or CSP, and is built on well-established principles of thermal power generation. A significant portion of the world's electricity is generated through thermal power conversion. Most thermal power production worldwide is based on either the Rankine cycle or, to a lesser extent, the Brayton cycle. Both of these cycles are applicable to solar thermal power conversion, with the Rankine cycle being the more prevalent choice. Typically, water serves as the working fluid for the Rankine cycle. However, for lower-temperature solar collection systems ranging from $70°C$ to about $300°C$, organic fluids are employed, leading to the designation of the cycle as the organic Rankine cycle (ORC). When a Rankine cycle operates under supercritical conditions of the working fluid, it is referred to as the supercritical Rankine cycle (SRC). The Stirling cycle has also demonstrated significant potential, and solar thermal power systems based on this cycle are actively under development. More recently, researchers have been exploring modifications of these cycles, entirely new cycles, or combined cycles to enhance conversion efficiencies and adapt them more effectively to solar collection systems [9].

5.1.1 Organic Rankine Cycle

The majority of currently operational thermal power plants are founded on the Rankine cycle. The organic Rankine cycle (ORC) is based on the principles of the steam Rankine cycle but employs organic working fluids with lower boiling points to harness heat from heat sources operating at lower temperatures. The fundamental ideal Rankine cycle is illustrated in the Figure 5.1, which also provides a temperature-entropy (T-s) diagram depicting steam as the working fluid.

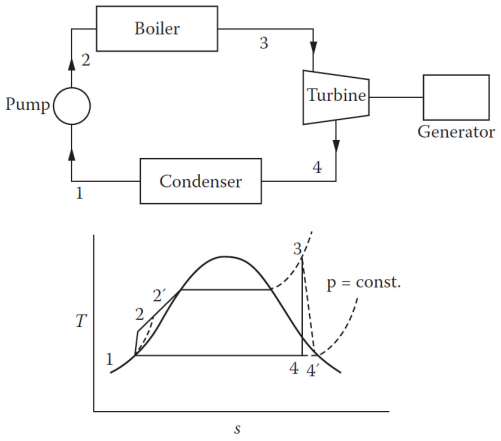

Figure 5.1: Basic Rankine Power Cycle [9]

The ideal Rankine cycle follows these primary processes:

- $1 \rightarrow 2$: Saturated liquid from the condenser at state 1 is isentropically pumped to the boiler at state 2.
- $2 \rightarrow 3$: Liquid is heated in the boiler at a constant pressure. The temperature of the liquid increases until it reaches the point of becoming a saturated liquid. Further heat input leads to the vaporization of the liquid at a constant temperature until the entire liquid phase is converted into saturated vapor. Any additional heat input superheats the working fluid to reach state 3.
- $3 \rightarrow 4$: Steam expands isentropically through a turbine, reaching state 4.
- $4 \rightarrow 1$: The steam exiting the turbine undergoes condensation at constant pressure until it returns to state 1 as saturated liquid.

5.2 Working fluid classification

Unlike the traditional Rankine cycle, which exclusively employs water as the working fluid, there exists a multitude of organic fluids suitable for use in Organic Rankine Cycles (ORC_s). These various working fluids possess distinct physical properties that can significantly influence the efficiency of the ORC system, the dimensions of its components, system stability and safety, as well as environmental considerations.

For instance, the critical temperature and the normal boiling point of a working fluid dictate the operational temperature range of the system. Thermal conductivity plays a role in determining the required heat transfer area for heat exchangers. Furthermore, factors like the ozone depletion potential (ODP), global warming potential (GWP), and atmospheric lifetime (ALT) can impact whether a specific working fluid complies with environmental regulations and standards.

Hence, the selection of working fluids is a critical aspect of ORC system design. Typically, in the quest for a suitable working fluid, designers and engineers rely on heuristic guidelines, drawing from their expertise and knowledge to identify a list of potential candidate working fluids. Subsequently, each of these candidate working fluids undergoes an evaluation process involving the optimization of operating parameters for the predefined cycle configuration. When necessary, component selection and sizing are conducted to assess the overall system's economic viability. Ultimately, the choice of appropriate working fluids is determined based on the outcomes of these evaluations. [6]

5.2.1 Type of Organic Working Fluid

Organic working fluids can be categorized into three types based on the slope of their saturated vapor curve: dry fluid, isentropic fluid, and wet fluid Figure 5.2.There are several ways to categorize organic fluids, but the most crucial classification is determined by the slope of the saturated vapor curve. This classification significantly impacts the efficiency of the Rankine cycle, the suitability of the fluid for various applications, and the characteristics of the plant components.

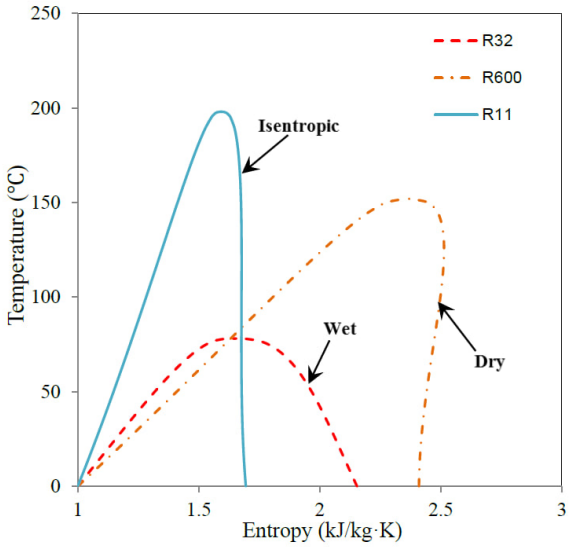

Figure 5.2: Three Types of Organic Working Fluid. [21]

The degree of wetness or dryness of a fluid is quantified by the inverse of the slope, denoted as $\xi = ds/dT$. Consequently, a positive value of ξ indicates a dry fluid, $\xi \sim 0$ characterizes an isentropic fluid, and $\xi < 0$ signifies a wet fluid. So We see three saturation curves:

- R11: Isentropic fluid with a positive slope of the upper limit vertical curve.

- R32: Wet fluid with a negative slope of the upper limit curve, similar to that of water. During the isentropic expansion in the turbine, condensate is formed.
- R11: Dry fluid with a positive slope of the upper limit curve. In this case, isentropic expansion leads to the superheated vapor region.

Wet fluids generally have relatively low critical temperatures, which necessitate the use of very high expansion pressures to enhance cycle efficiency. To achieve this, one or more superheating stages are often required to prevent condensation in the final stages of the turbine. While this plant configuration yields good efficiencies, it is not cost-effective.

In contrast, the use of dry or isentropic fluids eliminates the need for superheating, as superheated vapor is obtained at the outlet of the isentropic turbine. Additionally, a regenerator can be implemented to harness the thermal energy of the superheated vapor by heating the fluid exiting the pump. Another benefit of using organic working fluids is that ORC systems typically require a single-stage expander in the turbine, which leads to a simpler and more cost-effective system in terms of both initial capital expenses and maintenance. [12]

5.2.2 Influence of latent heat, density and specific heat

To enhance the performance of an organic Rankine cycle system, it is advantageous to use a working fluid with high latent heat, high density, and low liquid specific heat. A fluid with these characteristics can absorb more energy from the heat source in the evaporator, resulting in a reduction in the necessary flow rate, the overall size of the facility, and the power consumption of the pump.

The specific heat of the liquid does not influence the net work output extracted from the cycle. On the other hand, the specific heat of the vapor does affect the cost of the evaporator because a low value increases the required exchange area. Thermal conductivity also plays a role in the size of the air exchanger. In particular, higher thermal conductivity results in more efficient heat exchange in heat exchangers, reducing the required exchange area. Therefore, for the same mechanical power output from the turbine, fluids with higher latent heat, producing more specific work, require a lower mass flow rate and the selected fluid needs to have the highest possible density in both liquid and vapour phases. Having a high liquid phase density reduces pumping losses, while a high vapor phase density reduces pressure losses in the heat exchangers. [12]

5.2.3 Viscosity

Understanding the fluid viscosity is essential because it influences heat transfer and pressure losses in the pipes. The heat transfer coefficient can be expressed as:

$$h = \frac{Nu \cdot k}{d} = \frac{0.023 Re^{0.8} \cdot Pr^{n} \cdot k}{d} \tag{5.1}$$

$$Re = \frac{\rho \cdot u \cdot d}{\mu} \tag{5.2}$$

$$Pr = \frac{\mu \cdot c_p}{k} \tag{5.3}$$

As per equation Equation (5.2), we understand that the Reynolds number is inversely related to viscosity (μ). Furthermore, in accordance with equation eq. (5.3), the Prandtl number is directly related to viscosity. Equation eq. (5.1) indicates that viscosity has a direct relationship with the heat transfer coefficient. Consequently, when viscosity increases, the heat transfer coefficient also increases.

The distributed pressure losses in a pipe are:

$$\Delta P = \frac{f \cdot L \cdot \rho \cdot u^2}{2d} \tag{5.4}$$

Where f represents the friction factor, and its relationship with the Reynolds number is inverse, meaning it's directly linked to viscosity. Consequently, lower viscosity leads to reduced pressure losses and a decrease in the heat transfer coefficient. [12]

5.2.4 Stability of the fluid and compatibility with materials in contact

In contrast to water, organic fluids tend to experience chemical degradation and decomposition at elevated temperatures. Therefore, the highest allowable operating temperature is constrained by the chemical stability of the working fluid. Moreover, the chosen working fluid should be non-corrosive and compatible with the materials of the engine and lubricating oil.

It is also necessary to conduct compatibility tests between the fluid and the materials in contact to prevent excessive maintenance of the system. [12]

5.2.5 Environmental aspects

Regarding environmental aspects, the primary concerns include the ozone depletion potential (ODP), global warming potential (GWP), and the atmospheric lifetime (ALT). ODP and GWP reflect a substance's potential to contribute to ozone degradation and global warming. In response to environmental concerns, some working fluids have been phased out, such as R-11, R-12, R-113, R-114, and R-115, while others are scheduled to be phased out in 2020 or 2030 (e.g., R-21, R-22, R-123, R-124, R-141b, and R-142b).

Alternative fluids are being sought and applied, with the aim of retaining favorable properties and avoiding adverse environmental impacts. The most promising candidates are still found among fluids that contain fluorine and carbon atoms. The inclusion of one or more hydrogen atoms in the molecule leads to significant degradation in the lower atmosphere due to naturally occurring hydroxyl radicals, ensuring that only a small portion of the fluid persists and enters the stratosphere [12]

5.2.6 Safety

The ASHRAE refrigerant safety classification provides a valuable indication of the fluid's potential danger level. In general, it is desirable for fluids to possess characteristics such as non-corrosiveness, non-flammability, and non-toxicity. However, these attributes may not always be practically attainable or absolutely necessary. For instance, substances like R-601 are classified as flammable, but this is not a concern if there are no ignition sources nearby. Nevertheless, auto-ignition can be problematic, especially for longer alkanes at temperatures exceeding $200°C$.

Additionally, it is important to consider factors like the maximum allowable concentration and explosion limits. [12]

5.2.7 Critical points of the working fluids

Condensation is an essential process in both the organic Rankine cycle and supercritical Rankine cycle. The design condensation temperature is typically set above 300 K to dissipate heat to the surrounding environment. The critical point of a working fluid, which marks the peak of the fluid's saturation line on a T-s diagram, provides guidance for the suitable operating temperature range for the liquid and vapor forms of the working fluid. The critical temperature is a crucial parameter for selecting the fluid.

Another significant thermodynamic property is the freezing point of the fluid, which must be lower than the lowest operating temperature within the cycle. The fluid also needs to operate within an acceptable pressure range. Extremely high pressures or high vacuums can negatively affect the cycle's reliability or increase costs. [12]

5.3 Energetic Analysis

In this section, an energy analysis of the Rankine cycle is undertaken to enhance understanding of the formulas utilized in the plant engineering segment. There are various plant solutions employed for ORC cycles:

- Simple Rankine cycles, as previously introduced;
- Recovery or regenerative Rankine cycles, featuring a recuperator positioned between the turbine and the condenser;
- Double-expansion Rankine cycles with a direct heat exchanger recuperator;
- Organic flash cycle, where the fluid undergoes expansion through a flash tank, generating a vapor fraction that enters the turbine for power generation, while the liquid fraction bypasses the turbine;
- Trilateral Cycles (TLC), expanding the two-phase mixture

During the discussion, two specific types of plants will be examined from the aforementioned options: the simple Rankine cycle and subsequently the regenerative cycle, with a focus on explicating their plant engineering and energy characteristics. [4]

5.3.1 Basic cycle

A baseline cycle is selected for the computation of the necessary input and output powers of the system. The pressure losses at both the evaporator and the condenser are regarded as insignificant.

In a practical Rankine cycle, the pumping and turbine expansion processes deviate from the idealized ones. The reference point 1 represents the initial conditions of the fluid, which is compressed to point 2 to reach the desired pressure. Knowing the flow rate of the cycle, the power supplied to the feed pump is:

$$W_{\mathbf{p,id}} = \dot{m} \cdot (h_{2,id} - h_1) \tag{5.5}$$

The real power absorbed thanks to the pump efficiency (η_p) is determinated by:

$$W_p = \frac{W_{\mathbf{p,id}}}{\eta_p} \tag{5.6}$$

The power supplied to the evaporator and the power released to the condenser are:

$$Q_{\mathbf{eva}} = \dot{m} \cdot (h_5 - h_2) \tag{5.7}$$

$$Q_{\mathbf{cond}} = \dot{m} \cdot (h_6 - h_1) \tag{5.8}$$

The mechanic efficiency generated by the turbine is derived as:

$$W_{\mathbf{t,id}} = \dot{m} \cdot (h_5 - h_{6,id}) \tag{5.9}$$

Thanks to the isentropic efficiency ($\eta_{t,is}$) of the turbine it is possible to calculate the real power produced:

$$h_6 = h_5 - \eta_{t,is} \cdot (h_5 - h_{6,id}) \tag{5.10}$$

$$W_t = \dot{m} \cdot (h_5 - h_6) \tag{5.11}$$

The total cycle efficiency turns out to be:

$$\eta_{\mathbf{orc}} = \frac{W_{\mathbf{net}}}{Q_{\mathbf{eva}}} = \frac{W_t - W_p}{Q_{\mathbf{eva}}} \tag{5.12}$$

The efficiencies attained by the organic Rankine cycle can surpass 15%. Despite not being high, it's crucial to acknowledge that these cycles utilize low-temperature heat, which is more readily available. To enhance efficiency further, regenerative Rankine cycles are utilized. [4]

5.3.2 Regenerative cycle

Another enhancement to the fundamental Rankine cycle is the regenerative cycle, where expanded steam is extracted at multiple points in the turbine and blended with condensed water to preheat it in the feedwater heaters.

Figure 5.3 provides a schematic diagram and the Figure 5.4 a $T - s$ diagram of a Rankine cycle with regeneration.

Incorporating the heat exchanger enables a lower temperature at the condenser inlet and a higher temperature at the evaporator inlet, resulting in savings in the thermal power that must be supplied.

To calculate the power absorbed by the pump, we utilize equations Equation (5.5) and Equation (5.6). The exchanged power is determined based on the efficiency of the regenerator ($\eta_{\mathbf{r}}$).

$$Q_{\mathbf{reg,max}} = \dot{m} \cdot (h'_5 - h_{2a}) = \dot{m} \cdot (h_{4a} - h_{2a}) \tag{5.13}$$

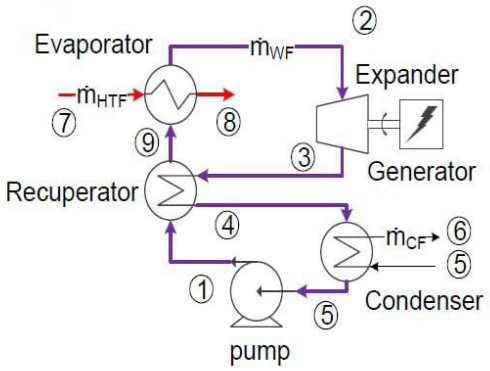

Figure 5.3: ORC with recuperator cycle layout [4]

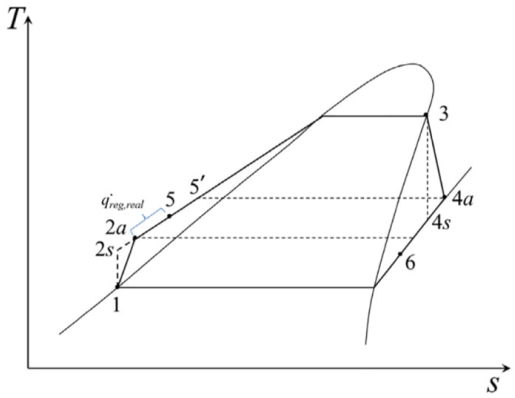

Figure 5.4: ORC with recuperator T-s diagram [30]

$$\eta_{\mathbf{r}} = \frac{Q_{\mathbf{reg}}}{Q_{\mathbf{reg,max}}} = \frac{h_5 - h_{2a}}{h_{4a} - h_{2a}} \tag{5.14}$$

$$Q_{\mathbf{reg}} = \eta_{\mathbf{r}} \cdot Q_{\mathbf{reg,max}} = \eta_{\mathbf{r}} \cdot \dot{m} \cdot (h_{4a} - h_{2a}) \tag{5.15}$$

The power to the evaporator and condenser are:

$$Q'_{\mathbf{eva}} = \dot{m} \cdot (h_3 - h_5) \tag{5.16}$$

$$Q'_{\mathbf{cond}} = \dot{m} \cdot (h_6 - h_1) \tag{5.17}$$

The power generated by the turbine is then computed as the relation in Equation (5.9), Equation (5.10) and Equation (5.11) considering the new points 3,4a,4s. Therefore, the efficiency of the regenerative cycle is:

$$\eta\mathbf{orc} = \frac{W\mathbf{net}}{Q'_{\mathbf{eva}}} = \frac{W_t - W_p}{Q'_{\mathbf{eva}}} \tag{5.18}$$

$Q'_{\mathbf{eva}}$, in the regenerative case, is lower than $Q_{\mathbf{eva}}$, calculated in the previous paragraph. From the efficiency formula, it is evident that reducing the power at the evaporator while maintaining

the same net power output increases efficiency. Despite the efficiency improvement, the system's complexity rises, and adding another heat exchanger could negatively impact investment costs. For smaller-scale plants, a simpler configuration is preferred. It is crucial to evaluate whether the energy savings in economic terms outweigh the installation cost of an additional heat exchanger [4].

5.3.3 Supercritical Rankine cycle

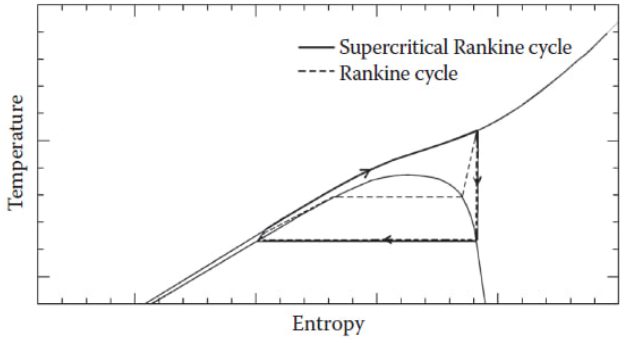

Figure 5.5: A supercritical Rankine cycle on a T-s diagram

Traditional Rankine cycles typically operate under subcritical conditions and use pure working fluids. However, using a pure fluid can lead to a temperature profile mismatch with the heat source, since the pure fluid boils at a constant temperature fig. 5.5, resulting in increased losses in the heat exchange process. This issue can be mitigated through the use of a Supercritical Rankine Cycle (SRC).

In an SRC, the working fluid is pressurized beyond its critical pressure and then heated isobarically, transitioning it directly to the supercritical vapor phase. The supercritical vapor is subsequently expanded in the turbine, generating mechanical work. The turbine's exhaust is then cooled to return the fluid to a liquid state in a condenser, and the condensed fluid is pumped back to high pressure.

While a steam Rankine cycle can also be operated under supercritical conditions, steam's critical pressure is notably high, necessitating specific material requirements that increase costs. In contrast, organic fluids like hydrocarbons and refrigerants have lower critical temperatures and pressures, making them attractive options for SRC_s, especially for low and medium temperature heat sources. These organic fluids offer improved efficiency in SRC_s compared to conventional Organic Rankine Cycles (ORC_s) [4].

5.4 Difference with the tradional Rankine Cycle

In traditional CHP (Combined Heat and Power) plants, particularly those employing the Rankine cycle, water serves as the working fluid. However, the characteristics and limitations associated with water necessitate extreme thermal conditions, leading to heightened plant complexity,

increased investment, and elevated costs. The reliance on high heat sources for heat-to-power conversion further compounds the challenge, and such intense heat sources are often unavailable in nature or environmentally benign. Despite these challenges, water, as a working fluid, proves to be an ideal steam when considering the humidity range on a TS-diagram. Water is readily available, cost-effective, environmentally friendly, non-toxic, emits non-harmful substances, and does not contribute to increased ozone depletion potential (ODP) or global warming potential (GWP), making it a favorable choice.

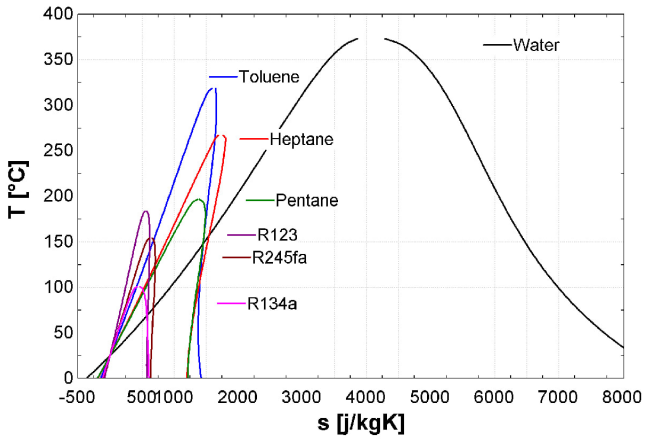

Figure 5.6: T-s diagram of a few typical organic fluids and of water [22]

In Figure 5.6, the T-s diagram illustrates the saturation curves of water and several typical organic fluids utilized in ORC applications. Two primary distinctions can be observed: [4]

1. The saturated vapor curve's slope (right curve of the dome) is negative for water, whereas it is more vertical for organic fluids. Consequently, the restriction on vapor quality at the end of the expansion process is eliminated in an ORC cycle, eliminating the need for vapor superheating before entering the turbine.

2. The entropy difference between saturated liquid and saturated vapor is significantly smaller for organic fluids. This results in a smaller enthalpy of vaporization. Therefore, for the same thermal power through the evaporator, the mass flow rate of the organic working fluid must be much higher than that of water, leading to increased pump consumption.

5.4.1 Low temperature heat recovery

Because organic working fluids have a lower boiling point, they enable the recovery of heat at much lower temperatures. This capability facilitates power generation from sources such as geothermal heat [4].

5.4.2 Component Size

The dimensions of the components are strongly influenced by the volume flow rate of the working fluid, as pressure drops escalate with the square of the fluid velocity. Consequently, there is a need

to enhance the hydraulic diameter of heat exchangers and the diameter of pipes to mitigate this velocity. The size of the turbine is approximately proportional to the volume flow rate [4].

5.4.3 Tubrine inlet temperature

In steam Rankine cycles, meeting the superheating requirement necessitates a turbine inlet temperature exceeding $450°C$ to prevent the formation of droplets during expansion. This results in elevated thermal stresses on the boiler and turbine blades, leading to increased costs. [4]

5.4.4 High Pressure

In a steam cycle, pressures typically range from 60 to 70 bar, leading to increased complexity and cost of the steam boiler due to thermal stresses. In an ORC, pressures generally do not exceed 30 bar. Additionally, the working fluid is not directly evaporated at the heat source (e.g., a biomass burner) but through an intermediary heat transfer loop. This simplifies heat recovery, as thermal oil operates at ambient pressure, eliminating the need for an on-site steam boiler operator [4].

5.4.5 Condensing Pressure

To prevent air infiltrations in the cycle, it is recommended to have high condensing pressures. Unlike water, which generally has a condensing pressure lower than 100 mbar absolute, low-temperature organic fluids meet this requirement by condensing at a pressure higher than atmospheric pressure. However, fluids with a higher critical temperature, such as hexane or toluene, are subatmospheric at ambient temperature [4].

5.4.6 Fluid Characteristics

tilizing water as a working fluid offers several advantages compared to organic fluids. Its key benefits include:

- Cost-effectiveness and widespread availability
- Non-toxicity
- Non-flammability
- Environmentally friendly: low Global Warming Potential (GWP), and zero Ozone Depleting Potential (ODP)
- Chemical stability: no working fluid deterioration in the case of hot spots in the evaporator
- Low viscosity: resulting in lower friction losses and higher heat exchange coefficients

Hower friction losses and higher heat exchange coefficients However, steam cycles are generally not completely sealed, leading to water loss due to leaks, drainage, or boiler blowdown. Consequently, a water treatment system must be integrated into the power plant to supply the cycle with high-purity deionized water. [4]

5.4.7 Turbine design

In steam cycles, the pressure ratio and the enthalpy drop on the turbine are both very high. This involves using turbines with several expansion stages. In ORC cycles the enthalpy drop is much lower, and single or two-stage turbines are usually used, which reduces their cost. Additional effects of the low enthalpy drop include lower rotating speeds and lower tip speed. The lower rotating speed allows direct drive of the electric generator without reduction gear (this is especially advantageous for low power-range plants), while the low tip speed decreases the stress on the turbine blade and makes their design easier [4].

5.4.8 Efficiency

The efficiency of existing high-temperature Organic Rankine Cycles (ORCs) does not surpass 24%. Conversely, conventional steam Rankine cycles exhibit thermal efficiencies exceeding 30%, albeit with a more intricate cycle design in terms of the number of components or size. This pattern also holds true for low-temperature heat sources, where steam Rankine cycles maintain higher efficiency compared to ORC cycles [4].

Chapter 6

Modelling

This chapter describes the process of sizing a system that aims to produce an electrical power output of 10 kW. The system layout involves analyzing different organic fluids for energy production and selecting the most suitable one based on its GWP and ODP indices.

The sizing process begins with the ORC cycle, which employs a cascade methodology in reverse until reaching the CSP system. Once the working fluid is chosen, the Rankine cycle will be sized by determining the flow rate necessary to produce 10 kWe of power. The working conditions of the heat transfer fluid will be selected based on the power generated at the evaporator. Finally, the CSP system will be sized, taking into account the daily electrical energy requirement. All the models are created using the Aspen Plus software.

6.1 Solar Dish Concentrator

The concentration system examined in this study is a disc-based parabolic solar collector situated on the rooftop of the Energy Center in Turin. The paraboloid was specifically designed and constructed by El.Ma. srl Electronic Machining in collaboration with the Polytechnic University of Turin. Its purpose is to facilitate laboratory experiments for research objectives and temporary applications. The disc concentrator, illustrated in fig. 6.1, comprises an aluminum paraboloid internally coated with a reflective polymer film known for its high optical efficiency. Additionally, the system is integrated with an automatic solar tracking mechanism featuring two independent axes (azimuth and elevation). This configuration ensures the reception of solar radiation at the most advantageous angle of incidence. Through real-time calculations of solar coordinates, the tracker dynamically aligns the system with the sun, optimizing its orientation moment by moment. The paraboloid boasts a capturing surface of 4.5 m^2 with an optical efficiency of 80% , and temperatures of up to 1800°C can be attained at the focal point of the parabola.

Starting from the seasonal average temperature radiation, in the Figure 6.2 are represented the temperatures reached at the focus of the paraboloid.

6.2 ORC Cycle

In this thesis, we opted to employ the solar concentrator detailed in the preceding section to drive the ORC cycle. This decision has implications for the choice of fluids used within the cycle. As

Figure 6.1: Solar concentrator produced by Em.Ma. srl Electronic Machining and installed on the roof of the Energy Center.

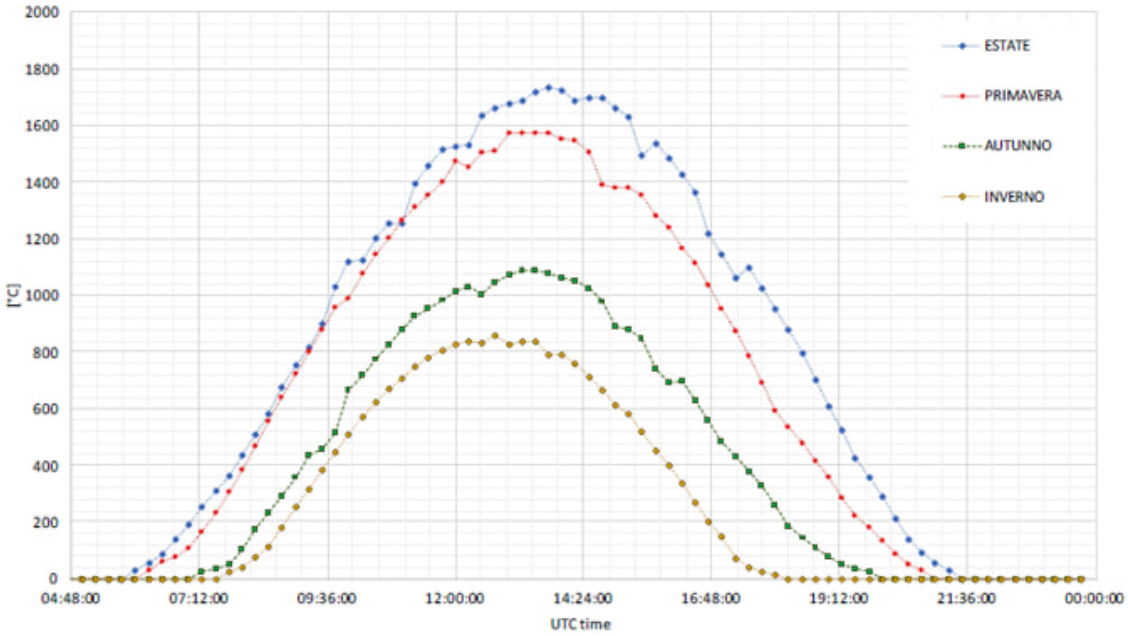

Figure 6.2: Daily variation of the seasonal average temperature reached at the focus of the parabola.

illustrated in Figure 6.2 , the disc concentrator enables the attainment of elevated temperatures at the parabola's focal point (surpassing 1700°C). However, it is crucial to not only consider the temperatures reached but also the duration for which these temperatures can be sustained each day.

The effectiveness of the organic Rankine cycle (ORC) is contingent upon the fluid temperature in the paraboloid surpassing a specific threshold temperature established for each fluid during the sensitivity analysis of the evaporator.

The choice of working fluid is a crucial aspect in the design of the ORC. When selecting a working fluid, various criteria must be taken into account, including environmental sustainability, ozone depletion potential (ODP), global warming potential (GWP), safety (non-flammable, non-toxic, and non-corrosive properties), vapor pressure in the boiler, critical temperature, and thermal stability. It is clear that nowadays there is a growing interest in enviromentally more sustainable working fluids.

During the discussion, an examination was carried out on six organic fluids within a pressure range of 1 to 10/14 bars (depending on the examined fluid). The fluids examined will be presented in the following table:

Substance	Chemical formula	Critical Temperature ($^\circ C$)	Critical Pressure (bar)	Normal boiling point ($^\circ C$)	Type	ODP	GWP
Toluene	$CH_3C_6H_5$	318.60	41.08	110.60	Dry	0	3
R-141b	CH_3CCL_2F	204.35	42.12	32.05	Isentropic	0.11	> 600
Heptane	$CH_3(CH_2)_5CH_3$	267.05	27.4	98.42	Dry	0	< 6
Pentane	$CH_3(CH_2)_3CH_3$	196.55	33.7	36.06	Dry	0	< 6
Hexane	$CH_3(CH_2)_4CH_3$	234.45	30.25	68.72	Dry	0	3
R-245fa	$C_3H_3F_5$	154.5	36.4	15.29	Isentropic	0	> 800

Table 6.1: Organic fluids characteristics

The Table 6.1 indicates that the working conditions specified for each fluid do not surpass the critical pressure value. After determining the maximum working conditions for the fluid, the plant conditions are then established, considering machine efficiency, as well as the initial temperature and pressure.

6.2.1 Basic cycle

Using the ASPEN PLUS software we were able to individually analyze all organic fluids for the sizing of the machines in the simplest cycle, as we can see in the Figure 6.3 below.

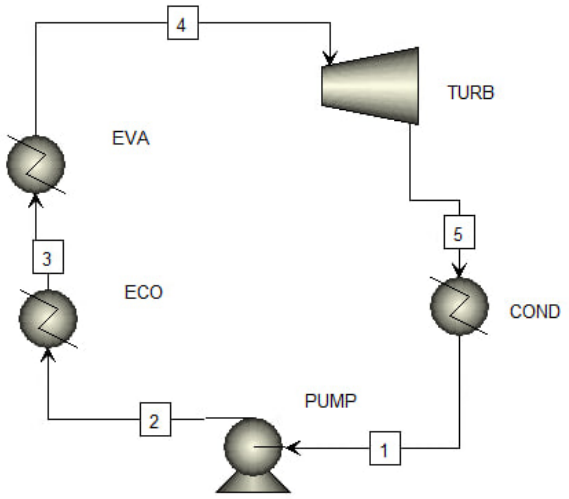

Figure 6.3: Basic Rankine Cyel on ASPEN PLUS

For each unit were established the operating conditions:

- Pump: increase in pressure to allow the transition within approximately 30% of the critical pressure;
- Economizer and Evaporator: together represents the heat exchanger block. They works at high pressure with imposed outlet condition of total steam at the evaporator outlet;
- Turbine: discharging in pressure to the initial value of pressure;
- Condenser: it takes back the fluid to the initial condition at 1 bar and 25°C.

After acquiring the power data for the evaporator, pump, turbine, and condenser, the cycle's efficiency was assessed using Equation (5.12). The results obtained will be presented upon completion of the discussion on the regenerative Rankine cycle.

6.2.2 Recuperative cycle

In the regenerative scenario, outlined in Section 5.3.2, a heat exchanger is positioned downstream of the turbine to preheat the fluid prior to its arrival at the evaporator.

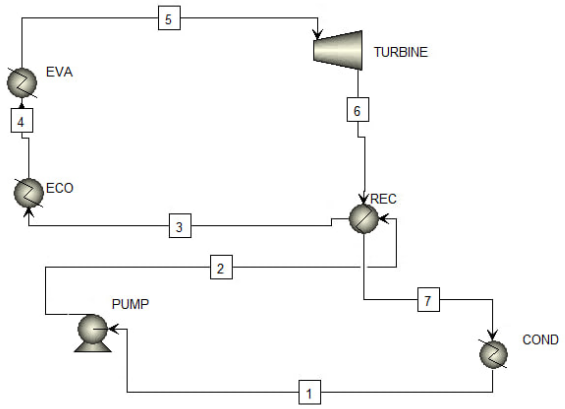

Figure 6.4: Regenerative Rankine cycle ASPEN PLUS

This configuration is expected to exhibit higher efficiency in comparison to the simpler case. Conditions largely remain consistent with the simple case, except for the regenerator, which necessitates input data for software operation. The regenerator is conceptualized as a countercurrent exchanger, aiming to enhance heat exchange and yield greater advantages than the straightforward case. It is crucial for the steam fluid condition at the turbine exit to remain unchanged even following the heat transfer to the regenerator (point 3). For the efficiency calculation, reference is made to Equation (5.18).

6.3 Fluid selection

In this section, for the optimal selection of the organic fluid to consider in our project, several fluids have been evaluated under their optimal operating conditions. The fluids were examined within their respective cycles as shown in the preceding paragraphs (section 6.2.1 section 6.2.2), using the Aspen Plus software. This approach allowed us, under the same conditions, to identify the fluid that, from a technical perspective, may represent the best choice, taking into account factors such as efficiency within an organic Rankine cycle, the power required by the cycle components, and consequently the power produced as a function of the flow rate. Some fluids, under identical conditions, require lower flow rates to produce the same amount of power. As shown in Section 6.2, both purely synthetic fluids, such as R141b and R245fa, belonging to the category of Hydrofluorocarbons (HFCs), and Hydrocarbons (HCS) such as Toluene and Pentane, etc., have been examined [5]. Both categories of fluids can be obtained synthetically in the laboratory; however, what characterizes compounds like Toluene, is the possibility of finding it directly in nature within other sources such as crude oil. This will affect some fundamental parameters that have been considered in the choice of the fluids themselves.

After exporting the data for each fluid, a comparison is made to select the fluid with the most favorable properties regarding power requirements at the evaporator and cycle efficiency. The graph below provides a summary of the efficiencies achieved in both the simple and regenerative scenarios.

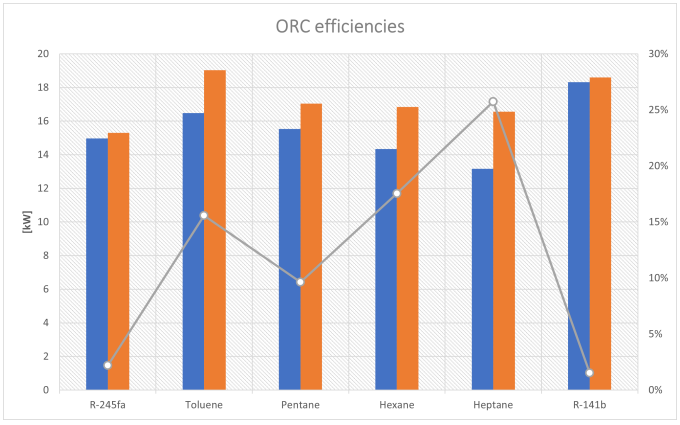

Figure 6.5: Comparison of the organic fluids efficiencies (basic cycle in blue, regenerative in orange

Through Figure 6.5, we can obtain a comparison via percentage values between the simple organic Rankine cycle and the regenerative one, highlighting the improvement for each considered fluid. All fluids show a percentage improvement of at least 10%, except for the two synthetic fluids which, due to lower power produced in the turbine, do not exhibit a significant improvement at the same evaporator required power.

The power absorbed at the evaporator for each organic fluid is readily provided:

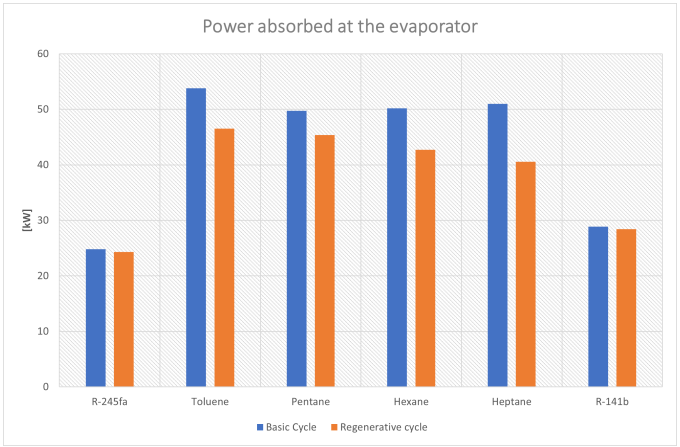

Figure 6.6: Evaporator power of the organic fluids

From the Figure 6.6, a clear difference in power required at the evaporator between synthetic and natural organic fluids is intuitively noticeable. The former have a significantly lower power requirement due the lower boiling point as reported in Table 6.1. These data, along with the

efficiency values, are crucial for selecting a fluid that delivers the required power to the expander net of a low power demand at the evaporator. Or rather, this is the most favorable condition; it is equally important, therefore, to also consider the net power produced under the same conditions fig. 6.7:

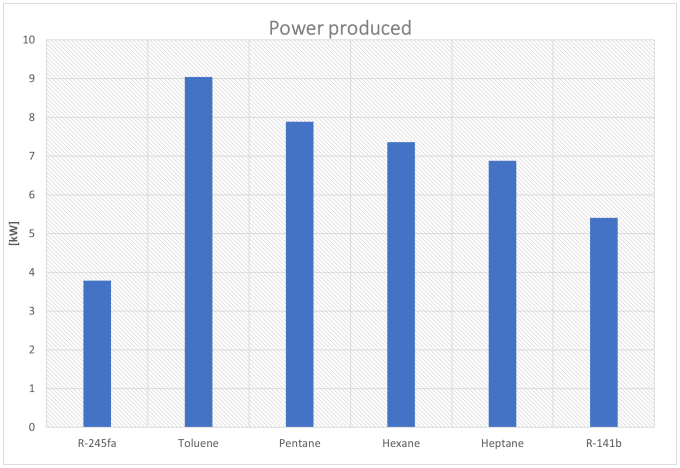

Figure 6.7: Produced power by the organic fluids

Natural organic fluids, at the same flow rate, produce more power due to their higher molecular weight. In other words, to generate a certain power, a lower flow rate of natural organic fluid will be needed compared to a synthetic fluid.

In conclusion, natural organic fluids exhibit higher power output but also greater evaporator demand, whereas synthetic ones exhibit the opposite trend. The discriminating parameter would then be the cycle efficiency value, but as mentioned in previous paragraphs (6.2), it is also important to evaluate environmental impact parameters. In the cases examined, R-141-B and Toluene are the two fluids with the best parameters considered for synthetic and natural organic fluids, respectively. However, considering a zero ODP since it is natural and a significantly lower GWP, Toluene emerges as the preferred organic fluid. Despite Toluene having higher critical temperature values compared to the synthetic fluid for comparison, a choice in favor of environmental impact index was preferred, even to diverge from the more common refrigerants used in the market. Toluene indeed has a critical temperature that makes it one of the best fluids for high-temperature (HT) scenarios [31]. However, as observed in Figure 6.2, the paraboloid achieves influential temperatures, which could represent an excellent case study.

6.4 Sensitivity analysis and operating point o the system

In this paragraph, all components of the Organic Rankine Cycle (ORC) are analyzed, starting from the turbine and reaching the downstream evaporator of the plant. To analyze each component, it was chosen to vary parameters within a arbitrarily chosen range in order to observe the behavior of other fundamental parameters of the component. The only fixed parameter of the project, as agreed upon in the initial project choices, is the power output from the turbine as well as its electrical energy production, set at 10 kWe.

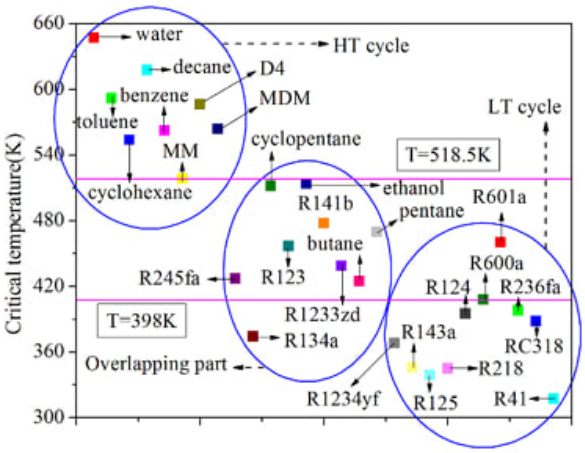

Figure 6.8: The critical temperature for different working fluids in the HT and LT cycle. [31]

6.4.1 Turbine

Starting from the expander, it is studied as per choice with Toluene as the refrigerant fluid. To examine its behavior and identify the optimal operating point, the power output value is set at 10 kWe and the fluid's inlet temperature is fixed. The choice of the output power has already been justified, while the decision to impose the inlet temperature in the turbine for Toluene was evaluated based on the physical characteristics of the refrigerant fluid. The inlet temperature was limited in such a way as to have a value that simultaneously did not reach the critical temperature value of the fluid and allowed the fluid to reach the vapor state without the presence of liquid particles, therefore decided also for the safety of the system.

To complete the cycle modeling using Aspen Plus, the isentropic and mechanical efficiency of the turbine, as well as the efficiency of the alternator responsible for converting the produced energy into electrical energy, were also assumed. The preset values are represented in the following table:

Parameter		**Value**	**[SI Unit]**
Inlet Temperature	$T_{in,turbine}$	300	$°C$
Inlet Pressure	$P_{in,turbine}$	32	bar
Vapor fraction	χ	1	
Isentropic efficiency	$\eta_{is,turbine}$	0.9	
Mechanic efficiency	$\eta_{mech,turbine}$	0.98	
Mechanical power output	$W_{out,turbine}$	10	kW
Alternator efficiency	η_{al}	0.98	
Electric power otuput	W_{el}	9.8	kWe

Table 6.2: Parameters set for modeling the turbine in the ORC cycle.

To model the component in the Aspen Plus software, a compressor named "Pressure Changers" was used, to which, through the software's function option, it was specified to operate as a turbine. Once the input values for the software were determined, the optimal fluid flow rate

was searched based on the turbine's outlet pressure. The outlet pressure value from the turbine is a crucial value to be sought so that there is a slightly higher outlet pressure than the atmospheric pressure, in order to avoid air infiltration into the plant. The flow rate values, on the other hand, were varied starting from a base value of 0.1 kg/s up to an arbitrary value of 1.5 kg/s with increments of 0.01 kg/s for each iteration.

In our case, as shown in the fig. 6.9, Toluene reaches optimal turbine outlet pressure values already with the minimum flow rate considered. As the curve itself suggests, an increase in flow rate corresponds to an increase in pressure; however, maintaining a higher pressure level could result in operational issues or simply require more effort in terms of work from components such as the pump.

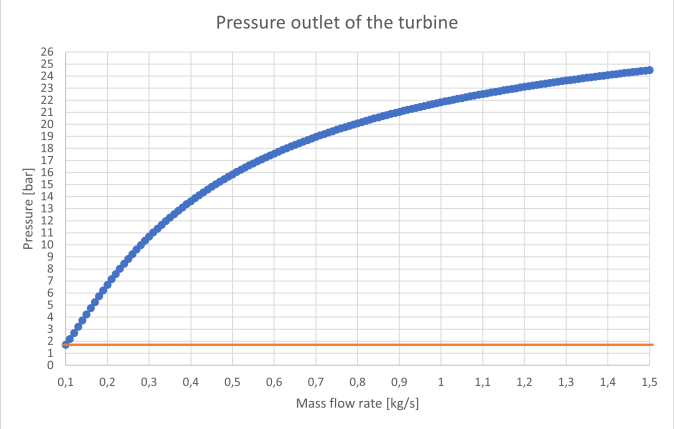

Figure 6.9: Temperature outlet from the turbine to a pressure level of about 1 bar for Toluene

Therefore, it was decided to operate according to the initially set flow rate value, which allows the cycle to function while obtaining an outlet pressure value that prevents air infiltration. The chosen point, intersected in the figure by the horizontal line, has the following parameters:

Parameter		**Value**	**Si Unit**
Outlet Pressure of Turbine	$P_{out,turbine}$	1.7	bar
Mass flow rate	$\dot{m}_{orc}$	0.1	kg/s

Table 6.3: Fixed parameters for the Turbine

In conclusion, the Aspen Plus software shows us (fig. 6.10) the values of the temperature exiting the expander and the corresponding vapor fraction, which allows us to ensure that we are in a condition of pure vapor, necessary to avoid the formation of liquid particles in the turbine that could compromise its operation.

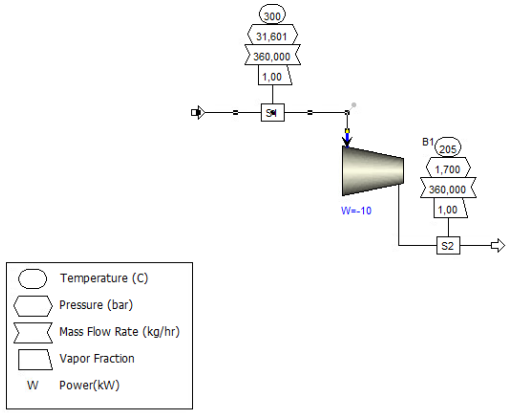

Figure 6.10: Aspen Plus scheme with output values

6.4.2 Condenser

Following the ORC cycle, the exhaust steam exiting the turbine must be processed through a condenser to allow the continuation of the cycle. The condenser acts as a counter-flow heat exchanger through which the working fluid circulating within our ORC cycle (Toluene), acting as the hot fluid that needs to release heat, and the cold refrigerant fluid that absorbs the heat released by the Organic Rankine Cycle fluid. The cold fluid entering the secondary circuit of the condenser thus facilitates the transition of the working fluid from a vapor to a liquid state, allowing it to start a new Rankine cycle and move on to the next component. Conversely, the cold fluid, by absorbing the heat released by the hotter fluid, exits the condenser at a higher temperature. This temperature can be utilized since the cycle has been designed following a cogeneration production of both electrical and thermal energy. Therefore, water has been chosen as the cold fluid entering the condenser, which, upon exiting at an appropriate temperature, will be able to utilize this absorbed heat in various applications.

Through Aspen Plus, it was possible to model this sensitivity analysis using the Heat Exchanger as the component for the condenser. The parameters set for launching the analysis are the mass flow rate value, as described in the evaporator analysis, and in general, the parameters at the outlet of the preceding component, i.e., the turbine, were kept constant. The following table indicates:

Parameter		**Value**	**SI Unit**
Inlet Temperature of Toluene	$T_{cond,in}$	205	$°C$
Inlet Pressure of Toluene	$P_{cond,in}$	1.7	bar
Outlet Pressure of Toluene	$P_{cond,out}$	1.7	bar
Inlet Temperature of Water	$T_{H_2O,in}$	60	$°C$
Inlet Pressure of Water	$P_{H_2O,in}$	1	bar

Table 6.4: Fixed parameters for the condenser

As previously, using the software, the missing values at the outlet of the component were

obtained, including the outlet temperature of the water and its flow rate. A sensitivity analysis is then conducted to obtain the optimal point between the two parameters. Through the "Sensitivity" tool, the water flow rate is varied from 0.1 kg/s to 2 kg/s with an increment of 0.1 kg/s, and for each iteration, the software is asked to determine the outlet temperature of the refrigerant fluid, water in our case.

The process results is showed in fig. 6.11.

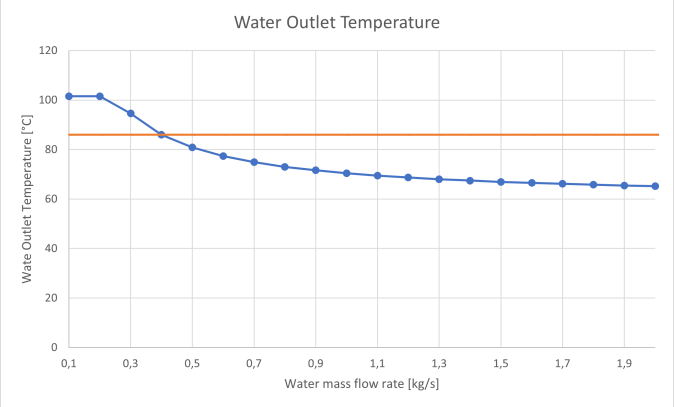

Figure 6.11: Outlet Temperature of the Water from the condenser as a function of the flow rate

Considering the design choice of a cogeneration plant, capable of producing thermal energy through the waste heat at the condenser, the optimal operating point chosen is where the outlet water temperature reaches a sufficiently high value relative to the flow rate used, in order to exploit its absorbed heat at the outlet. As depicted in the fig. 6.11, the values of the chosen optimal point are reported in the table 6.5:

Parameter		**Value**	**Si Unit**
Outlet Temperature of Water	$T_{out,turbine}$	86	$°C$
Mass flow rate	$\dot{m}_{h_2o}$	0.5	kg/s

Table 6.5: Output parameters from sensitivity analysis

The fig. 6.12 below shows the model diagrammed in Aspen Plus with the values obtained from the software, including the heat recovered from the condenser and the null vapor fraction at its outlet, ensuring complete condensation of the hot fluid.

So we recover a thermal power from the condenser like in the table 6.6.

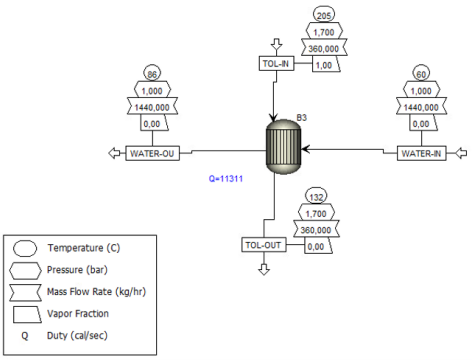

Figure 6.12: Aspen Plus scheme with output values

	Parameter	Value	Si Unit
Thermal Power	$W_{th,out}$	47.4	kW_{th}

Table 6.6: Output power from sensitivity analysis

6.4.3 Pump

Through the pump, the liquid fluid exiting the condenser undergoes a pressure increase necessary for the subsequent evaporation process. As a standard procedure for the sensitivity analysis of the component, the inlet conditions obtained from the outlet conditions of the condenser (fig. 6.12) were set using Aspen Plus. The other parameter set to proceed with the software is the isentropic efficiency of the pump and the outlet pressure value equal to that obtained at the inlet of the evaporator.

In the fig. 6.13, we notice how the temperature undergoes a slight increase due to the irreversibilities of the pump. Furthermore, the power of the pump, which will impact the final power balance, is seen to be a value almost negligible compared to the power produced by the expander.

The values obtained are then reported in the table 6.8.

Parameter		Value	SI Unit
Inlet Pressure of Toluene	$P_{pump,in}$	1.7	bar
Outlet Pressure of Toluene	$P_{pump,out}$	32	bar
Isentropic efficiency	η_{is}	0.9	

Table 6.7: Fixed parameters for the pump

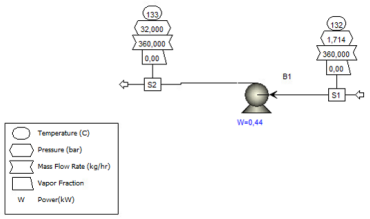

Figure 6.13: Aspen Plus scheme with output values

6.4.4 Heat Transfer Fluid

Before analyzing the heat exchange component, namely the evaporator, it was necessary to choose a heat transfer fluid that represents the 'hot fluid' in the heat exchange process.

Heat transfer fluids are essential in indirect power production, as they transfer heat to water inside the heat exchanger. The steam generated from this heat is then directed to the turbine for power generation. The turbine requires a minimum rated pressure of fluid to operate effectively. Therefore, it's crucial to achieve the desired pressure and temperature when the heat is released from the heat transfer fluid (HTF) in the heat exchanger. Several criteria must be considered when selecting an appropriate HTF, including the following:

- High operating temperature
- Stability at high temperature
- Low material maintenance and transport costs
- Non-corrosive
- Safe to use
- Low vapor pressure
- Product life cycle
- Low freezing point
- Low viscosity

Based on the specified selection criteria, heat transfer fluids commonly employed in concentrated solar power systems have been evaluated, and several options have been identified along

	Parameter	Value	SI Unit
Outlet Temperature of Toluene	$T_{pump,out}$	133	$°C$
Power required by the pump	$W_{el,pump}$	0.44	kW_{el}

Table 6.8: Output parameters of the pump

with their properties sourced from various literature sources. Among the currently utilized heat transfer fluids, phenyl-naphthalene has emerged as the top performer following performance assessment [26].

HTF	$T_{max}[K]$	$C_p[kJ/kgK]$	$\rho[kg/m^3]$	$K[W/mK]$	$\mu[mPa\dot{s}]$
Phenyl-naphthalene	600	2.6	849	0.077	0.11

Table 6.9: *Source: NREL, ORNL for Heat Transfer Fluids

6.4.5 Evaporator

The last component of the cycle to be subjected to sensitivity analysis is the Evaporator. The evaporator is the main component of the system that connects the Organic Rankine Cycle with the energy transport cycle in the form of heat from the solar concentrator.

The evaporator is a heat exchanger traversed by two counter-current flows, similar to the condenser, a hot fluid and a cold one. According to the second law of thermodynamics, the hot fluid is tasked with transferring the heat it carries to the cold fluid, which in turn absorbs the transferred heat. In this case, the hot fluid is represented by the heat transfer fluid (HTF) circulating within the coils placed in the receiver of the paraboloid, while the cold refrigerant fluid is the fluid circulating in the Organic Rankine Cycle, namely Toluene. The heat transfer fluid used to model the system is the Phenyl-naphthalene as described in section 6.4.4.

On Aspen Plus, the HeatX component from the Exchangers library was utilized, and the parameters set for the design conditions of the component correspond to the values of the flows obtained from the pump analysis model. Other assumptions include maintaining a constant pressure within the heat exchange process and ensuring that the exit temperature of the refrigerant fluid matches the one set as the inlet temperature to the turbine.

	Parameter	Value	SI Unit
Mass flow rate	$\dot{m}_{orc}$	0.1	kg/s
Inlet temperature	$T_{eva,in}$	62	$^{\circ}C$
Inlet pressure	$P_{eva,in}$	32	bar
Outlet pressure	$P_{eva,out}$	32	bar
Outlet temperature	$T_{eva,out}$	300	$^{\circ}C$

Table 6.10: Fixed parameters for Evaporator

To achieve these predetermined values at the outlet, the hot HTF fluid must be capable of supplying heat starting from a naturally higher temperature. Therefore, the following values have been decided:

	Parameter	Value	SI Unit
Inlet temperature of HTF	$T_{HTF,in}$	400	$^{\circ}C$
Inlet pressure of HTF	$P_{HTF,in}$	3.2	bar

Table 6.11: Fixed parameters of the HTF fluid

To determine the flow rate of the heat transfer fluid, a sensitivity analysis is required to determine the variation in the outlet temperature of the fluid as a function of the flow rate. The flow rate was varied from a base value of 0.2 kg/s to a maximum value of 2 kg/s, with increments of 0.1 kg/s per iteration. Analyses below the minimum value of 0.2 kg/s were excluded as they caused crossover issues in the software. The chosen optimal point was the one capable of ensuring a temperature difference between the inlet and outlet, and a flow rate value that could facilitate the evaporation process without the use of excessive flow rates. The determined values are:

	Parameter	Value	SI Unit
Outlet Temperature of HTF	$T_{HTF,out}$	353	$°C$
Mass flow rate of HTF	$\dot{m}_{HTF}$	0.5	kg/s

Table 6.12: Output parameters of the HTF fluid

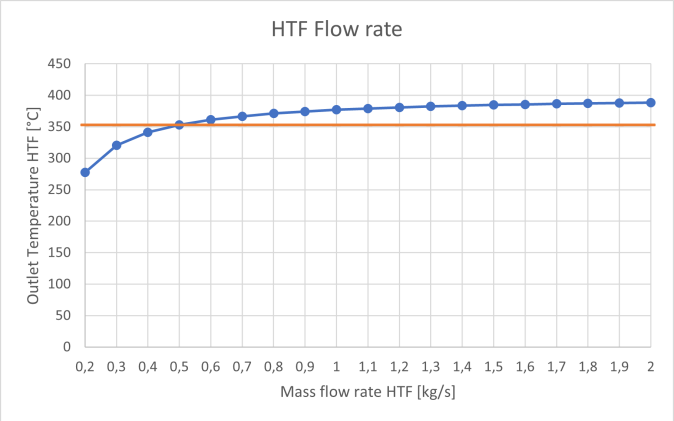

Figure 6.14: HTF Mass flow rate as a function of the outlet temperature

The thermal power required for the evaporation of the refrigerant fluid is reported in the table 6.13.

	Parameter	Value	SI Unit
Evaporator thermal power	$W_{th,in}$	70.47	kW_{th}

Table 6.13: Output parameters of the HTF fluid

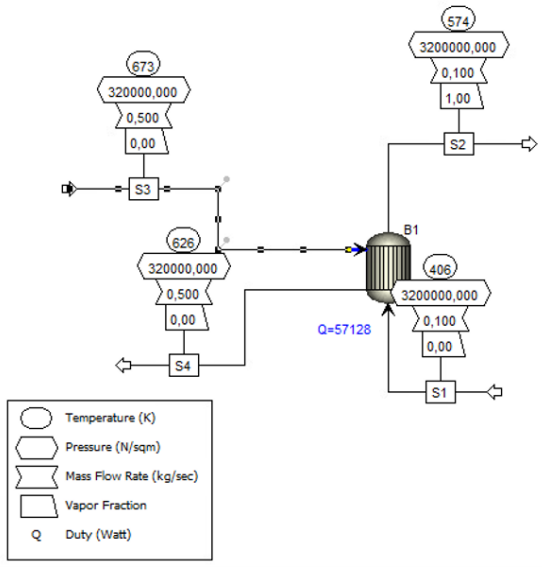

Figure 6.15: Aspen Plus scheme of the Evaporator

6.5 Basic ORC cycle

After modeling each component according to its optimal operating point, it is possible to assemble the entire cycle with the appropriate fluids considered. Below are the fluids with the obtained key points and the complete scheme using Aspen Plus.

The fig. 6.16 depicts the organic Rankine cycle modeled with the operating fluid Toluene. The two main curves, labeled as LLC and ULC, represent the lower and upper limit curves, distinguishing the phases change zones of the fluid. The numbers represent the milestones identified through modeling, and the key points indicated exactly mark the entry and exit points of the components along the cycle.

The shown phases represent:

- $1 \rightarrow 2$: It represents the pumping phase to reach the operating pressure before entering the evaporator. The temperature rise is minimal, so the points appear to coincide;
- $2 \rightarrow 4$: It represents the evaporation phase where the fluid enters in part from milestone 2 into the evaporator and is then heated through the economizer still in liquid phase until milestone 3, subsequently in the section up to milestone 4, the final evaporation process occurs where the fluid also undergoes a phase change to vapor state;
- $4 \rightarrow 5$: This segment represents the expansion phase within the turbine. The process is not perfectly isentropic due to the irreversibilities of the system;

Figure 6.16: ORC cycle with Toluene in T-s diagram

- $5 \rightarrow 1$:The last segment between landmarks 5 and 1 represents what happens inside the condenser. The condensation process brings the vapor fluid through an initial cooling process to landmark 6, where we reach saturated vapor condition on the upper boundary curve. In conclusion, the fluid continues to release heat until returning to landmark 1, where the phase change to liquid state is completed.

The final cycle modeled using Aspen Plus software is depicted in fig. 6.17, producing a predetermined power output of $10kW$ ($9.8kW_{el}$) at the turbine and a thermal output of $47.3kW_{th}$.

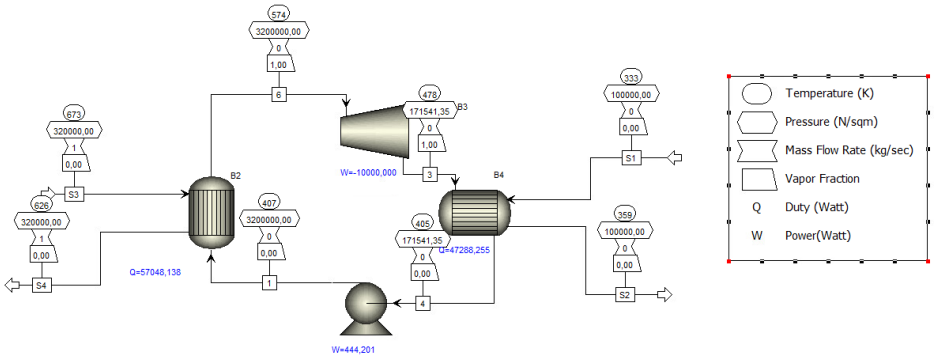

Figure 6.17: Basic ORC

6.6 Regenerative ORC cycle

To analyze other plant configurations, we chose to model the cycle in its regenerative variant, including a recuperator, in order to attempt to improve its efficiency.

The recuperator is a simple heat exchanger that allows us to preheat the liquid exiting the pump before entering the evaporation process, using part of the sensible heat recovered from the exhaust steam exiting the expander. This mechanism enables us to have a lower power demand at the evaporator, which will deal with a fluid at a higher inlet temperature, closer to steam conditions. Consequently, this will result in a reduced demand from the solar field, translating into a decrease in the surface area used and therefore the number of collectors required. As it's still an energy balance, the portion of heat we recover will be subtracted from the heat recovered at the condenser.

Using the software, we decided to keep the same data as for the simple cycle, with the addition of the recuperator, and let the software provide us with the results through simulation. In conclusion, we obtained a recovery heat of approximately $8.9kW$ and a consequent reduction in thermal recovery at the condenser to 38.4 kW, leading to a lower evaporative demand of about $48.1kW$ as shown in the fig. 6.18.

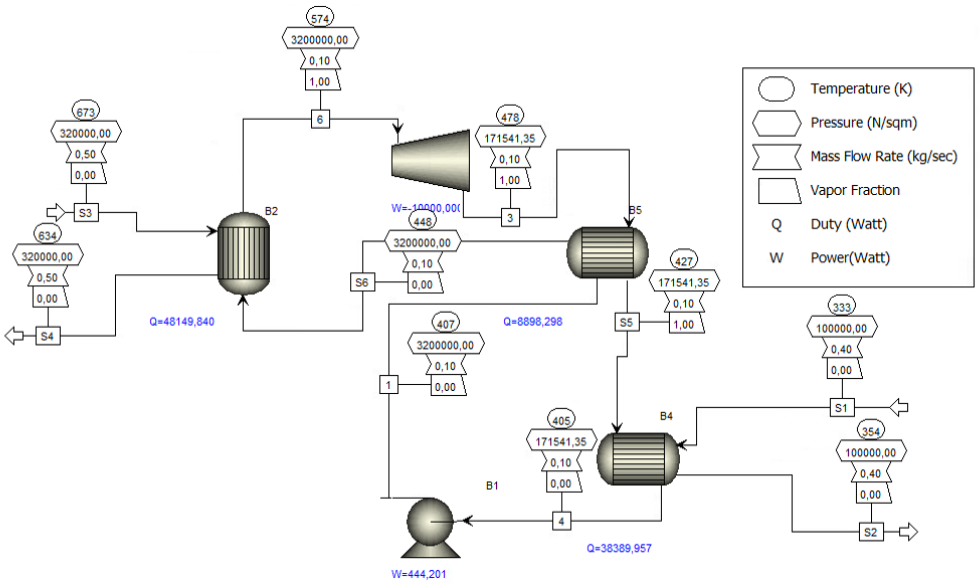

Figure 6.18: Rigenerative ORC

In the representation on the diagram as a function of temperature and specific entropy, we notice how the recuperator allows the fluid to enter the evaporation process from a much higher temperature, represented by point $2'$, without the use of external heat sources but solely by exploiting the sensible heat recovered from the exhaust steam of the turbine. The diagram depicts the organic Rankine cycle, with the thermal recovery process shown by the dashed line.

The phases of the cycle are:

- $1 \rightarrow 2$: It corresponds to the pump operation segment, as in the simple case, the points appear to coincide due to the very low temperature rise;

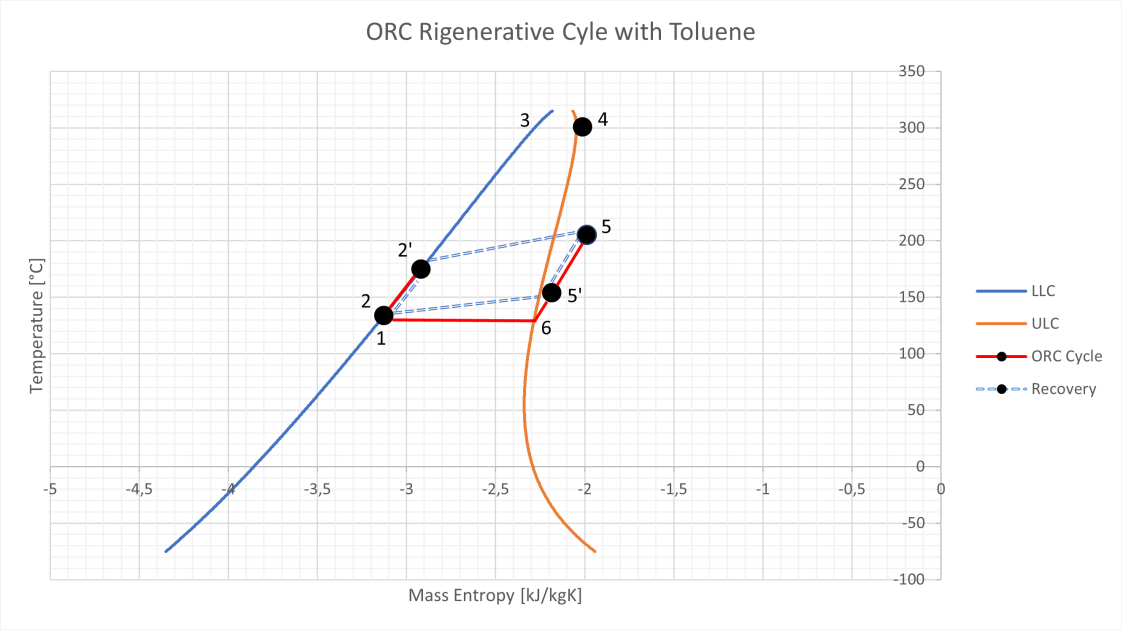

Figure 6.19: ORC cycle with Toluene in T-s diagram

- $2 \rightarrow 2' - 5 \rightarrow 5'$:These segments represent the work done by the recuperator. The heat recovered from the steam exiting the turbine enables the temperature jump between segments 2 and $2'$ of the liquid-state fluid. The heat facilitating this jump is instead represented by the release that occurs between segments 5 and $5'$;

- $2' \rightarrow 4$: This segment represents the work done by the evaporator, which, with the aid of the recuperator, starts its cycle from point $2'$. In the first segment between points $2'$ and 3, the fluid is heated while still in the liquid phase until it reaches the saturated liquid condition, then the evaporation process begins, culminating in the saturated vapor state represented by point 4;

- $4 \rightarrow 5$: This segment represents the work done by the expander, which takes the fluid from state 4 to state 5 through a decrease in temperature and pressure. The segment is not exactly isentropic due to system irreversibilities;

- $5' \rightarrow 1$: This is the final segment of the condenser, which returns the fluid to saturated liquid conditions, point 1, starting from cooling at constant temperature and pressure in the conditions of saturated vapor, in the segment between points $5'$ and 6.

6.7 Solar field

The organic cycle designed to produce a power output of 10 kWe must necessarily be supported by the energy input upstream of the solar concentrator. A single paraboloid, as currently situated on the roof of the Energy Center, is certainly not capable of providing the necessary heat to the heat exchanger to allow the cycle to operate according to these predetermined parameters. Therefore, in this section, we will model the solar field in order to determine how many parabolic solar concentrators will be needed for the organic Rankine cycle to produce the predetermined power output of 10 kWe. The procedure will be performed for both the simple Rankine cycle case and the case with a recuperator.

As expressed in section 6.4.4, the heat transfer fluid used is Phenyl-naphthalene, which will be tasked with absorbing energy in the form of heat provided by the concentration of solar radiation by the paraboloid, and then transferring it to the refrigerant fluid of the Rankine cycle through a heat exchanger. The parabolic concentrator will not reach the same temperature values at the focal point throughout the day but will vary depending on the variation of daily irradiance, which typically increases in the morning, peaks around noon, approximately at zenith, and then decreases towards the evening.

Analyzing these parameters to derive the temperature trend at the receiver's focal point will be important for the project, as our heat transfer fluid, to reach the predetermined temperature at the heat exchange in the evaporator, will need the solar concentrator to provide enough energy to reach the optimal temperature for the exchange. In other words, the Organic Rankine Cycle will only operate if the paraboloid reaches a minimum temperature at its focal point, allowing the HTF fluid to reach the desired temperature (set in table 6.11).

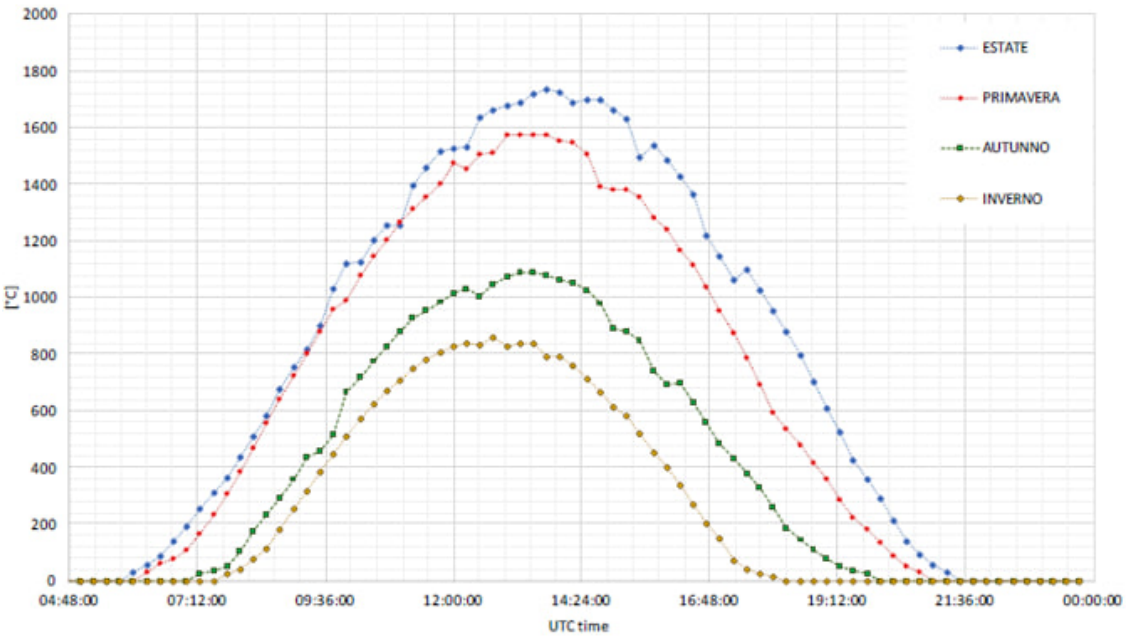

Figure 6.20: Daily variation of the seasonal average temperature reached on the focus of the paraboloid

The fig. 6.20 shows curves representing the daily variation of the seasonal average temperature, which, in relation to the horizontal line representing the temperature value required by the HTF, allows us to determine the daily operating hours of the cycle based on different seasons.

$T_{min} = 400°C$	**Time slot**	**Hours per season**
Spring	$08:00 - 18:55$	10.92
Summer	$07:50 - 19:40$	11.83
Autumn	$09:05 - 17:30$	8.42
Winter	$09:30 - 16:05$	6.58

Table 6.14: Cycle operating hours

Once the average daily operating hours were derived based on the season, the average seasonal direct normal irradiance (DNI) was calculated. This provides us with information regarding the radiation that will impact our parabolic concentrator during the hours when our cycle will be operational. To obtain this data, we utilized information from the meteorological station near the Energy Center, with data collected for the entire year of 2019. Direct radiation data was averaged over 15-minute intervals, and model days were selected for each season, representing optimal weather conditions without rain or data reception issues. It's worth noting that December 14 was used for the winter season due to unclear data availability for other winter days, making it the closest useful alternative.

Season	**Day**	$DNI[W/m^2]$
Spring	30-may	861.06
Summer	29-july	796.47
Autumn	04-november	610.39
Winter	14-december	718.3

Table 6.15: Direct Normal Irradiation for a reference day

Through the obtained seasonal average radiation, we can derive the annual average radiation as the average of the seasonal radiations, and consequently obtain the annual operating hours of the cycle, as well as the capacity factor.

Season	min per day	min per season
Spring	655.2	60278.4
Summer	709.8	66011.4
Autumn	505.2	44962.8
Winter	394.8	35137.2

Table 6.16: Average operating minutes per season

The equivalent annual operating hours with the ratio over the hours of an entire year (8760 h) are:

Parameter	Value	SI Uni
Annual operating hours	3439.83	h
Capacity factor	0.39	

Table 6.17: Annual operating hours

The annual average DNI, obtained from table 6.15 is:

Parameter	W/m^2
Annual DNI	746.56

Table 6.18: Annual Direct Normal Irradiation

For sizing the solar field, once the data for the annual average radiation is obtained, the thermal power data that the concentrating solar power plant must provide to the cycle need to be included. This is done in order to determine the area required for each parabolic trough to generate such power. The power produced by a single solar collector can be calculated using the formula:

$$Q_{csp} = DNI_{annual} \cdot \eta_{opt} \cdot A_{dish} \tag{6.1}$$

DNI represents the annual direct normal irradiance incident on the collector surface, cleaned by its optical efficiency, and then multiplied by the aperture area. According to the data from our installed parabolic trough, it has an area of $4.5m^2$ and an optical efficiency of 80 %, so each installed parabolic trough will generate a power of:

	Parameter	Value	SI Unit
Annual Direct Normal Irradiation	DNI_{annual}	746.56	W/m^2K
Optical efficiency	η_{opt}	0.8	
Area of a singol dish	A_{dish}	4.5	m^2
Thermal power of a single dish	Q_{csp}	2,69	kW

Table 6.19: Thermal power generated by a single parabolic collector

Knowing the values of the thermal power required by the evaporator to operate the cycle in both the simple and recuperated cases, it is therefore possible to obtain, through a simple ratio, the number of concentrating parabolic trough collectors needed to meet this requirement.

	Parameter	Value	SI Unit
Thermal power of basic cycle	$Q_{eva,b}$	57.05	kW
Thermal power of recuperative cycle	$Q_{eva,r}$	48.15	kW
Number of collectors for basic cycle	N_b	22	
Number of collectors for recuperative cycle	N_r	18	

Table 6.20: Number of collectors needed to satisfy the evaporator thermal request

It is also possible to convert these values into the total area of the solar field, in order to have a more 'universal' figure that can apply to any type of configuration that one may wish to install, regardless of the solar concentration system used. The result is obtained by equating the thermal power required by the evaporator with the power that the entire solar field should produce, and then deriving its area:

$$Q_{eva} = DNI_{annual} \cdot \eta_{opt} \cdot A_{solarfield} \tag{6.2}$$

	Variable	Value	SI Units
Solar field area for basic cycle	$A_{solarfield,b}$	95.52	m^2
Solar field area for recuperative cycle	$A_{solarfield,r}$	80.62	m^2

Table 6.21: Solar field area needed for satisfy the ORC cycle

The results show us how the case of the cycle with the recuperator indeed has its justification. The implementation of a heat recovery component allows us to have a lower heat demand at the evaporator, as the fluid will arrive with a higher temperature, resulting in a reduced need for solar collectors to be installed.

6.8 Discussion of the results

In this section, the results obtained considering the modeling of the system composed of the solar field and the Organic Rankine Cycle in its simple and regenerative cycle configurations will be discussed.

	Cycle	Parameter	Value	SI Unit
Power needed at the Evaporator	Basic Regenerative	$Q_{eva,b}$ $Q_{eva,r}$	57.05 48.15	kW
Power recovered at the Recuperator	Regenerative	Q_{rec}	8.9	kW
Power disposed at the Condenser	Basic Regenerative	$Q_{cond,b}$ $Q_{cond,r}$	47.29 38.39	kW

Table 6.22: All powers needed and recovered depending on the cycle

As mentioned earlier, when modeling the Organic Rankine Cycle, incorporating a recuperator helps to preheat the fluid entering the pump for the evaporation process. The recuperator utilizes the heat retained by the exhaust steam exiting the turbine. This results in a higher inlet temperature, which makes it easier for the evaporator component to function. As a result, the demand for thermal power is lower.

Conversely, as shown in table 6.22, the thermal energy we recover from the refrigerant fluid entering the condenser (water) will be lower compared to the modeling of the simple Organic Rankine Cycle. This is justified by the fact that the exhaust steam exiting the turbine will transfer some of its energy during the heat exchange in the recuperator and thus will be less efficient in the heat exchange with the water in the condenser, providing us with less recoverable energy that can then be used for other purposes.

As discussed in the thesis description, the plant modeling system was designed to produce electricity and heat simultaneously. This configuration was maintained in both the simple organic Rankine cycle and the regenerative case. By executing the cycle in the Aspen Plus software, we were able to determine the plant's efficiency in both configurations.

We calculated the efficiency of the entire plant using the values of irradiance captured by the paraboloids within the solar field and the output powers. We considered only the turbine power net of the pump as useful output power for the electricity produced. Alternatively, we also calculated the total efficiency of the cogenerative plant by including the thermal power as useful support from the condenser.

	Cycle	Parameter	Value	
Electrical efficiency of the plant	Basic Regenerative	$\eta_{el,b}$ $\eta_{el,r}$	13 15	%
Cogeneration efficiency of the plant	Basic Regenerative	$\eta_{cog,b}$ $\eta_{cog,r}$	77 79	%

Table 6.23: Efficiencies of the plant in his configurations

Based on the results obtained, the plant's modeling with regeneration indicates an improvement in efficiency, although the increase is not significant. Even though the regenerative cycle

provides less energy recovery from condensation, the use of the recuperator results in better co-generation efficiency. This is because it requires less power at the evaporator to compensate for the loss of recovered thermal energy at the condenser.

$$\eta_{el} = \frac{P_{el,t} - P_p}{DNI_{annual} \cdot N_c \cdot A_{dish}} \tag{6.3}$$

$$\eta_{cog} = \frac{P_{el,t} - P_p + P_{th,cond}}{DNI_{annual} \cdot N_c \cdot A_{dish}} \tag{6.4}$$

To calculate the efficiencies, the eq. (6.3) eq. (6.4) formulas shown above have been used. The useful power, including the thermal power recovered at the condenser for the case of the regenerative cycle, is compared to the input power represented by the average radiation incident on the solar field.

For the analysis of radiation in this study, the average radiation values for typical days of each season were used. This assumes a constant trend of performance throughout the cycle. In both the simple and regenerative cases, the production power has been set as a fixed value. Therefore, the cycle would perform with higher efficiency during times of the season when the incident direct radiation is lower. This is because lower incoming power would produce the same amount of electrical energy. However, this behavior is only possible in the case study. It is important to note that the electrical power output is assumed to be constant, and sunny days were considered without taking into account that the true operating hours of the system would decrease due to unfavorable weather conditions.

The other term introduced in the formula is the area of the solar field. In this case, the product of the area of a single parabolic trough (obtained as data from the component specifications) and the number of collectors previously calculated in table 6.20 was used. Since the number of required collectors is a rounded-up number due to the fact that the result of the calculated number of collectors was not a perfectly whole number, multiplying the rounded-up number of collectors by the area of a single parabolic trough will definitely produce an overestimated value of the area required for the solar field, thus contributing to limiting the efficiency values themselves. In conclusion, an evaluation could be made on how to best utilize the area of the solar field to introduce as few solar collectors as possible, thereby achieving economic savings, perhaps by using solar collectors with more compact geometries.

A possible implementation on the analyzed plant model could involve the system's operating hours. Previously, an operating time of the system of about 40% compared to the total available hours in a solar year was derived (table 6.17). Although this is not a very high value, it is worth considering that it is actually an overestimated value based on the assumptions made.

In fact, as already described, sunny days and "clear sky" conditions were used as sample days for each season, whereas on average throughout the year there is a frequency of precipitation ranging from 36 to 161 days ([25]), including days when solar radiation is covered by clouds.

This results in a very limited use of the cycle, which could instead operate continuously given the temperature levels it can reach at the focus of the parabolic trough.

In this regard, as briefly described in chapter 4, a storage system could be implemented to allow the system to store all the excess energy that could be obtained from the high temperature levels reached. Additionally, the thermal energy recovered at the condenser can serve various

functions. The production time slots are linked to the operation time slots of the cycle, which therefore correspond to the central periods of greatest availability of solar radiation.

During the colder seasons, there is a need for energy during the early morning and evening hours when residential heating systems are used. As a result, it is worth considering a storage system for the heated water exiting the condenser during these months. In contrast, during the warmer months, there is no need for heating, and the energy is required mostly during the central hours corresponding to the operating hours. Therefore, we can use it directly to produce cooling.

Chapter 7

Economic analysis

The economic analysis focuses on assessing the sustainability of a project by determining the costs involved in establishing a plant. By calculating different parameters, we can determine whether the project is technically feasible and economically sustainable, and whether it can recover the initial investment costs and generate reasonable profits in comparison to the market standards.

The economic analysis also helps in analyzing various aspects of the plant. By conducting investment analysis, we can identify opportunities to improve plant efficiency and operations by investing in certain components. The use of high-quality components may increase the overall plant performance, despite the higher costs involved.

In this final chapter of the plant analysis, we have evaluated the investment using various indices to determine the feasibility of the modeled plant. We have analyzed both simple and regenerative cases, assuming Toluene and Phenyl-Naphthalene as the operating and heat exchange fluids, respectively.

At the end of the analysis, we can determine whether the regenerative Rankine cycle case is more advantageous than the simple case in terms of economic feasibility, as observed in the modeling analysis.

It is important to note that the plant has been modeled for demonstration purposes, with a fixed electrical production of 10 kW and a heat recovery of about $38kW_{th}$ and $47kW_{th}$, respectively for the simple and regenerative cases.

7.1 Levels of Capital Costs

The methodology used for the analysis is based on that employed by NETL (National Energy Technology Laboratory), U.S. Department of Energy, which provides tailored guidelines for production plants and can also be applied to various types of generation plants (hydrogen, syngas generation, etc.). The costing methodology introduces specific capital cost levels on which NETL evaluates various production plants. The essential use of these standards allows for the comparison of different plant technologies on common criteria [20].

This methodology delineates capital costs into five levels:

1. **BEC** (Bare Erected Cost): includes expenses related to process equipment, on-site facilities, and infrastructure supporting the plant, such as shops, offices, labs, and roads, as well

as the direct and indirect labor needed for construction and installation;

2. **EPCC** (Engineering, Procurement, and Construction Cost): encompasses the BEC along with expenses for engineering, procurement, and construction (EPC) contractor services. EPC services comprise detailed design, contractor permitting, and project/construction management costs;

3. **TPC** (Total Plant Cost): consists of the EPCC plus project and process contingencies;

4. **TOC** (Total Overnight Capital): includes the TPC plus all other overnight costs, including owner's expenses;

5. **TASC** (Total As-Spent Capital): represents the sum of all capital expenditures incurred during the capital expenditure period, including their escalation and interest during construction.

BEC, EPCC, TPC and TOC are "overnight" costs and are expressed in "base-year" dollars. The base year is the first year of capital expenditure. TASC is expressed in mixed, current-years dollars over the entire capital expenditure period [20]. Overnight costs represents the costs that would occur if a project were to be implemented instantly, without taking into account any discount rate or inflation.

The Cost Estimate Classification System, as outlined in Recommended Practice 18R-97 by the Association for the Advancement of Cost Engineering International (AACE), is a framework used in Engineering, Procurement, and Construction within the process industries. The majority of techno-economic studies conducted by NETL utilize cost estimates tailored for "Feasibility Study" purposes, as per AACE Class 4 standards. Cost estimates in NETL studies typically have this following featyures [1]. It's useful to understand the range within the analysis conducted per this projects falls, with respect to the real value:

Project Definition	Typical Engineering Completed	Expected Accuracy
1 to 15%	• plant capacity, block schematics, indicated layout, process flow diagrams for main process • systems, and preliminary engineered process and utility • equipment lists	-15% to -30% on the low side, and +20% to +50% on the high side

Figure 7.1: Features of an AACE Class 4 Cost Estimate [1]

Therefore, the starting point of our economic analysis is the estimation of the BEC regarding all the components included in the cycle.

7.1.1 Estimation of the BEC

Based on the information provided by NETL in the purchased equipment section regarding the relationships and graphs used for determining capital costs, the program relies on a "module factor approach to costing" originally introduced by Guthrie and later modified by Ulrich. All the data reported stem from surveys on component manufacturing conducted from May to September 2001. With this information, we can adjust the relationships to current values based on the

Chemical Engineering Plant Cost Index (CEPCI), knowing the index value for 2001 and the present day [7].

The Chemical Engineering Plant Cost Index (CEPCI) is a benchmark value used for quickly assessing the equipment costs of a plant for chemical and industrial processes [16].

The cost of plant components depends on the operating parameters to which the component is subjected and the materials it is composed of. The cost functions used incorporate parameters that take into account both the construction materials and operating parameters such as operating pressure or other conditions depending on the component under consideration.

For components such as pumps and heat exchangers, the cost function used is as follows [7]:

$$C_{BEC} = C_p^0 \cdot (B_1 + B_2 \cdot F_M \cdot F_P) \tag{7.1}$$

where:

- C_p^0 is the purchasing cost of equipment referred to base conditions;
- B_1 and B_2 are constants correlated from data in previous work and are independent of the type of equipment;
- F_M is the material factor, which mainly depends on the operating temperature;
- F_P is the pressure factor, which depends on the operating pressure.

Data for the purchased cost of the equipment, at ambient operating pressure, were fitted to the following equation:

$$\text{Log}(C_P^0) = K_1 + K_2 \cdot \text{Log}(A) + K_3 \cdot [\text{Log}(A)]^2 \tag{7.2}$$

where:

- A is the capacity or size parameter of the equipment;
- K_1, K_2, and K_3 are constants that depend on the type of equipment involved.

Alternatively, the purchased cost can also be determined based on graphs that show the cost in dollars per size parameter, depending on the construction type of the component. All the parameters used in the equations shown can be obtained from graphs or tables that report values based on operating conditions, retrievable in Appendix A of the text [7]. Constants like $B1_1, B_2, K_1, K_2, K_3$ are determined based on the construction type of the component, while other parameters such as F_P and $F_M$are different from 1 in case the operating conditions are different from standard ambient conditions, so they will have specific relationships.

For components such as the turbine, not covered in the calculation relationship described above eq. (7.1), the cost function used will instead be:

$$C_{BEC} = C_P^0 \cdot F_{BM} \tag{7.3}$$

where F_{BM} is the Bare Module Factor that also considers the basic cost of the component beyond the material used.

Once the parameters are derived, it is possible to calculate the cost of the component relative to its size parameter. However, the relationships provided are often valid for size ranges different from those present in the model considered in the thesis project. Therefore, the use of the six-tenths rule [28] comes to aid, allowing us to adjust the cost of a component about the known cost of one of larger or smaller size:

$$\frac{C_1}{C_2} = \left(\frac{S_1}{S_2}\right)^{0.6} \tag{7.4}$$

where:

- C_2 is the cost evaluated with the given equation with size parameter S_2;
- S_1 is the size parameter of the real component.

Similarly, since the relationships are based on surveys from a specific period, they are functions of the reference year. Therefore, the CEPCI ratio is used to determine the cost of the component relative to the current year under consideration:

$$\frac{C_1}{C_2} = \frac{I_1}{I_2} \tag{7.5}$$

where :

- C_2 is the cost evaluated with the given equation at the CEPCI value for year I_2;
- I_1 is the CEPCI value for the year we are considering.

In our case, the CEPCI value of reference is at the year 2001 and 2023 for the year considered in the project. Values are taken from literature [16].

In conclusion, the derived values and respective key parameters for each component are presented:

Component	**Cycle**	C_P^0	C_{BEC}	**SI Unit**
Turbine	Basic Regenerative	14980,21	55426,77	$
Condenser	Basic Regenerative	3838,72 3946,94	17089,96 17571,75	$
Pump	Basic Regenerative	1261,9	5066,18	$
Evaporator	Basic Regenerative	3221,41 14700,03	3073,54 14025,25	$
Recuperator	Regenerative	3135,32	14307,17	$

Table 7.1: Puchased cost equipment

One of the final costs to consider is the expense of the parabolic concentrator and the alternator, which are significant components. The paragraph explains that the parabolic concentrator has a substantial cost and accounts for more than 70 percent of the total component costs. However, finding a specific price for the alternator that meets our plant requirements is difficult. Even though it is a less impactful expense, an approximate value has been estimated based on some alternators found in catalogs.

Component	Basic Cycle	Rigenerative Cycle	Unit
Parabolic collector	330000	270000	$
Alternator	≈ 200	≈ 200	$

Table 7.2: Purchased cost of equipment

The last costs are represented by the fluids used, the operating fluid of the Rankine cycle and the heat exchange fluid circulating from the solar collector. Knowing the flow rate, assuming an average operational time of 9.5 hours per day based on the previously derived seasonal average trend table 6.14, the purchase cost of the fluids used has been calculated according to their cost per metric ton (1000 kg):

Component	Flow rate $[kg/s]$	Cost [$\$/mt$]	Purchased cost [$]
Toluene	0.1	622	2127.24
Phenyl-napthalene	0.5	141.57	2420.85

Table 7.3: Purchased cost of the fluids

The values related to the costs per metric ton were obtained from literature.

7.1.2 Estimation of the EPCC

The cost estimates are based on an engineering, procurement, and construction management (EPCM) contracting strategy that involves multiple subcontracts. This strategy allows the owner to have better control over the project while minimizing or eliminating many of the risk premiums associated with lump sum EPC contracts. In a traditional lump sum EPC contract, the contractor assumes all risks related to performance, schedule, and cost. However, due to current market conditions, EPC contractors are less willing to bear extensive risk, and there's a trend towards a modified EPC approach in which the owner retains more risk. When contractors do agree to assume risks in lump-sum EPC contracts, it's reflected in the project cost. In today's market, contractors charge significant premiums for accepting these risks, particularly for performance risk, which can substantially inflate overall project costs [20].

Following the guidelines of NETL, EPCCs in this work are estimated at 8% of the BEC, so they have been calculated starting from the BEC of each component obtained in the previous step.

7.1.3 Estimation of TPC

Process and project contingencies are added to estimates to accommodate anticipated yet unspecified costs resulting from incomplete project definition and engineering. These contingencies

are included because historical experience indicates that such costs are probable and anticipated, even though they cannot be precisely determined at the time of estimate preparation [20].

In our case, considering the commercial application of concentrated solar technology, the TPC is estimated to be 15% of the EPCC.

7.1.4 Estimation of TOC

In estimating the TOC, we consider:

- **Prepaid Royalties**, that in our case are included in the associated equipment cost and thus not included as a cost to the owner;
- **Preproduction (start-up) costs**, which include all the costs in order to do some preliminary tests and runs of the plant before starting. In our work, they're evaluated at 2 of TPC;
- **Working Capital** , although inventory capital (see below) is accounted for, no additional costs are included for working capital;
- **Inventory Capital** , which account for spare parts and fuel stocks. Since the fuel has a minor economic contribution, almost negligible, we only consider the spare parts portion, slightly increasing it to account for replacement and recirculation cases. So they're evaluated at 0.6% of TPC;
- **Land** , this is not included due to the solar collector we studied is already in a building owned by the Politecnico di Torino, and in general our purpose is to study a scenario that can be adapted on other sites;
- **Financing Cost**, 2.7% of TPC, this financing cost covers the cost of securing financing, including fees and closing costs but not including interest during construction;
- **Other Owner's Costs** , accounted for 10% of TPC.

In conclusion, we estimated a TOC total contributio of about $15{,}3\%$ of TPC [20].

7.1.5 Estimation of TASC

Concerning the TASC, they have been evaluated in case of Investor-Owned utility (IOU), that is suitable for smaller plants. The multiplyng factor to pass from TOC to TASC is 1.075 [20].

7.2 Evaluation of the Pay Back Time

Economic analysis methods are widely used for evaluating innovation projects. While these methods vary in implementation, they all follow the capital budgeting approach, which involves calculating the economic return of a project as a series of discounted cash flows. The Net Present Value (NPV) approach is perhaps the most popular and sophisticated economic valuation technique. It entails discounting all future cash flows, both inflows and outflows, resulting from the innovation project with a specified discount rate, and then aggregating them (see eq. (7.6)). The

merit of the innovation is assessed based on its contribution to generating economic value relative to the investment required [32]. Thanks to the NPV approach, we are able to evaluate the Pay Back Time too. Pay Back Time is the time needed to recover the initial investment during the lifetime of the project considered. In this project, we assumed a lifetime of 30 years [23].

$$NPV = -I + \sum_{t=0}^{n} \frac{NCF_t}{(1+i)^t} \tag{7.6}$$

Where NCF_t is the net cash flow generated by the project in year t and r is the discount rate.The discount rate is represented by an adjusted value that also takes into account risk factors such as inflation over the lifespan of the plant. The first principle of the NPV approach is that a Euro received in the future is worth less than a Euro received today due to the associated risk. Therefore, future cash flows are discounted annually. The discount rate represents the opportunity cost of the capital invested, which rises with the perceived riskiness of the innovation opportunity. Consequently, riskier projects are anticipated to yield higher returns. The second principle of the NPV approach is to consider all future net cash flows associated with the innovation opportunity [32].

The initial investment, considered in the NPV calculation, is represented by the capital costs derived from the previous section (section 7.1.5), obtained as TASC. Within this investment value, costs such as maintenance are also considered. This is useful for acknowledging that all costs are represented by the initial investment value, and during the years of the plant's lifetime, we will not have cash outflows, also thanks to the assumption that the only component requiring electrical power input, the pump, is self-sustained by a small portion provided by the expander.

It is important to define the incoming cash flows accurately. In our case, as self-consumers, we produce electrical and thermal energy instead of purchasing it from the grid. Therefore, the net incoming cash flow is represented by the economic savings we make by not buying from the market, but by relying on self-sufficiency. These savings should be considered for both electrical and thermal energy production.

$$S = (W_{el,t} - W_p) \cdot h_{ann} \cdot C_{el} + Q_{cond} \cdot h_{ann} \cdot C_{th} \tag{7.7}$$

Where C_{el} and C_{th} are the market price for electric and thermal energy. The annual cash flows (NCF_t), however, do not only take into account the savings we obtain by not purchasing from the grid, but in this thesis work, we also considered the incentives obtainable from the installation of certain types of plants, both from national and European funds.

7.2.1 Incentive

Funding renewable energy production facilities plays a crucial role in financing the global energy transition. Allocating funds towards the development and support of clean energy generation is one of the key steps to achieving the goals set in the energy transition. With this in mind, the thesis hypothesized that one can benefit from the incentives proposed according to European and national plans. There are various calls for which one can apply, with varying disbursement periods and deadlines for application. Each incentive has specific requirements and well-defined conditions for disbursement. For the plant modelled in this project, it was possible to verify compliance with requirements for incentives related to cogeneration plant production and the

production of energy from renewable sources for self-consumption to minimize dependence on the grid.

The Certificati Bianchi, also known as "Titoli di Efficienza Energetica" (TEE), are negotiable certificates that certify the achievement of energy savings in final energy uses through interventions and projects to increase energy efficiency. The white certificate system requires electricity and natural gas distributors to achieve annual energy savings targets, expressed in Tons of Oil Equivalent saved (TOE). The guide, prepared by GSE pursuant to the interministerial decree on the Certificati Bianchi (D.M. January 11, 2017, as amended by DM May 10, 2018), sets out the rules and obligations that obligated subjects must follow to request this type of Certificati Bianchi, which are useful for fulfilling the obligation. The energy efficiency projects that can be admitted to the mechanism are projects that have not yet been implemented and are capable of generating additional energy savings - lower energy consumption compared to that prior to the implementation of the measures or, in the case of new installations, lower than a reference consumption [18].

The Decree of 09/05/2011 clarifies that cogeneration units entered into operation since January 1, 2011, are considered CAR (High Efficiency Cogeneration) if they meet the requirements described below. CAR units are entitled to the issuance of the Certificati Bianchi, in a number commensurate with the primary energy saving achieved in the year, calculated as follows [17]:

$$RISP = \frac{E_{CHP}}{\eta_{E,RIF}} + \frac{H_{HCP}}{\eta_{T,RIF}} - F_{HCP} \tag{7.8}$$

Where:

- $RISP$, is the primary energy saving in MWh in a year;
- E_{CHP}, is the electric energy in MWh by cogeneration in a year;
- H_{CHP}, is the thermal energy in MWh by cogeneration in a year;
- $\eta_{E,RIF}$, is the average conventional efficiency of the Italian electricity generation fleet, assumed as 0.46;
- $\eta_{T,RIF}$, is the average conventional efficiency of the Italian thermal generation fleet, assumed as 0.82;
- F_{CHP}, is the fuel energy in MWh by cogeneration in a year.

In a year, the operator is entitlet to:

$$CB = RISP \cdot 0.086 \cdot K \tag{7.9}$$

Where $RISP \cdot 0.086$ is the saving expressed in TEP, K is a harmonization coefficient based on the installed electrical power (1.4 for plant under $1MW_e$). Certificati Bianchi are admitted, for our project, for 15 years for coegeneration plant from 2007 combined with district heating.

The economic valorization of Certificati Bianchi occurs through two possible methods (according to the mechanism introduced by D.M. 20 July 2004 and subsequent amendments, and the rules established by AEEG) [17]:

- Sale of TEEs to obligated subjects (through the dedicated market platform operating with periodic auction mechanisms or through bilateral negotiation).

- Purchase by G.S.E. at a predetermined price (for feb-2024, set at 273,15 $\$/tep$) [24].

In addition to the incentive of White Certificates, the Ministry of the Environment and Energy Security, in a cumulative manner, regulates the incentive methods to support electricity generated by renewable energy plants included in configurations of self-consumption for the sharing of renewable energy, defining criteria and concession methods. Beneficiaries are compensated in cases of self-consumption configurations for the sharing of renewable energy, applicable to renewable energy plants with a single plant capacity not exceeding $1MW$. Furthermore, the plants must meet performance and environmental protection requirements, including sustainability criteria. Assuming that these criteria also apply to the project at hand, the calculation of the premium tariff provides, for plants with a capacity of $200kW$ or less, a subsidy not exceeding $120\$/MWh$(in the case of photovoltaic plants, an additional correction of $10\$/Mwh$ is included). The period of entitlement to the incentivizing tariff starts from the date of commercial operation of the plant and lasts for 20 years, net of any shutdowns resulting from force majeure events or shutdowns made for the implementation of modernization and enhancement interventions that are not incentivized [19].

7.3 Levelized Cost of Electricity

The levelized cost of electricity (LCOE) is a measure that shows the average revenue per unit of electricity produced, which is necessary to cover the expenses of constructing and operating a power generation facility. It is calculated over an assumed financial lifespan and operational cycle. LCOE is a widely used metric to evaluate and compare the overall competitiveness of different power generation technologies. [8].

In this thesis project, electricity production has been regarded as a source of self-consumption; however, calculating the LCOE index is useful for making comparisons with market values and assessing the performance level of the plant in terms of the price at which we should sell the generated energy to recoup the investment. The calculation is based on the following formula:

$$LCOE = \frac{(1+i)^n \cdot i}{(1+i)^n - 1} \cdot \frac{C_{TASC}}{E} \tag{7.10}$$

The first fraction of the eq. (7.10) represents the so-called annuity factor, which allows for the calculation of the annual cash flow relative, in our case, to the total purchase cost (C_{TASC}), taking into account the discount rate (i) and the lifespan of the plant (n). In the denominator, the term E represents the quantity of net annual energy produced, which in the case of calculating the levelized cost of electricity is precisely represented by the net annual electrical energy. We can extend the relationship to also calculate the levelized cost of thermal energy and cogeneration of both.

7.4 Discussion of the results

Consolidating the results obtained in the previous chapter, below are the values obtained that allow us to evaluate the performance of the designed plant also from an economic standpoint, and thus its attractiveness as an investment.

Cost list				
	%	**ORC base**	**ORC rigenerative**	**Unit**
C_{BEC}	Components cost	426.262,9	380.377,1	$
C_{EPCC}	+ 8% C_{BEC}	460.363,9	410.807,7	$
C_{TPC}	+15%C_{EPCC}	529.418,53	472.428,34	$
C_TOC	+15,3% C_{TPC}	610.419,56	544.709,87	$
C_TASC	*1.075 C_{TOC}	656.201,03	585.563,11	$

Table 7.4: List of Capital Cost

Once the capital costs corresponding to the investment required for the project are obtained, as seen in table 7.4, and the savings obtained from both energy self-consumption and the incentives we can benefit from are calculated, as shown in table 7.5, it is possible to calculate the Net Present Value (NPV) of the investment regarding our plant. The Net Present Value, once it reaches a positive value, ensures the economic feasibility of the project with a consequent monetary return. The corresponding year to this event will consequently be the year of investment payback, that is, the moment when we economically recover the invested capital.

	Basic Cycle	**Rigenerative Cycle**	
Savings	18253.59	16569.8	$
Certificati Bianchi	8247.31	7128.61	$/y$
Decreto CER	23388.1	19714.35	$/y$

Table 7.5: Savings and Incentives

As noted in the fig. 7.2, it should be noted that the cash flows during the first 20 years are higher due to the incentives, but these incentives do not contribute throughout the assumed lifetime of the plant. However, this does not imply that the project is not profitable. Indeed, it still generates a positive net present value in the first 15 years and is sustained in the later years by energy self-consumption savings.

It is worth noting that, in this case, the simple cycle scenario reaches a higher net present value at the end of the plant's life cycle compared to the regenerative case, despite starting with a higher initial capital investment cost. This is because the simple cycle scenario generates higher cash flow inflows due to a greater contribution of thermal energy self-consumption from the condenser. In the regenerative case, some of that energy is utilized by the recuperator, which reduces the cash flow inflows. Similarly, incentives, which also act on the thermal energy contribution, will be lower for the regenerative case.

As shown in fig. 7.3 and fig. 7.4, both configurations of the cycle, simple and regenerative, achieve a positive Net Present Value by the 12th year of the plant's life, thus before the midpoint. It is observed that the curve exhibits a fairly linear trend for a significant portion of the plant's lifespan, followed by a decreasing trend towards the end of the plant's life. This is attributed, as mentioned, to the cessation of incentive contributions, which consequently reduce the cash flow inflows in the later years of the plant's life.

After calculating the amount of oil equivalent saved by the plant, we can also analyze the

	ORC Basic			ORC Rigenerative		
Year	Cah flows [$]	Discounted Cash flow	NPV [$]	Cah flows [$]	Discounted Cash flow	NPV [$]
0	/	-632812,9362	-632812,9362	/	-565848,7575	-565848,7575
1	49888,99812	50720,81956	-582092,1166	43412,76668	44136,60703	-521712,1504
2	49888,99812	51566,51033	-530525,6063	43412,76668	44872,5163	-476839,6341
3	49888,99812	52426,30168	-478099,3046	43412,76668	45620,69571	-431218,9384
4	49888,99812	53300,42871	-424798,8759	43412,76668	46381,34985	-384837,5886
5	49888,99812	54189,13045	-370609,7455	43412,76668	47154,68671	-337682,9019
6	49888,99812	55092,64991	-315517,0956	43412,76668	47940,91776	-289741,9841
7	49888,99812	56011,23415	-259505,8614	43412,76668	48740,25799	-241001,7261
8	49888,99812	56945,13435	-202560,7271	43412,76668	49552,92598	-191448,8001
9	49888,99812	57894,60589	-144666,1212	43412,76668	50379,14394	-141069,6562
10	49888,99812	58859,90838	-85806,21279	43412,76668	51219,1378	-89850,51839
11	49888,99812	59841,3058	-25964,90699	43412,76668	52073,13725	-37777,38114
12	49888,99812	60839,06649	34874,1595	43412,76668	52941,37581	15163,99467
13	49888,99812	61853,46329	96727,62278	43412,76668	53824,09091	68988,08558
14	49888,99812	62884,77357	159612,3964	43412,76668	54721,5239	123709,6095
15	49888,99812	63933,27935	223545,6757	43412,76668	55633,92019	179343,5297
16	41641,68762	54254,02971	277799,7054	36284,1524	47273,81609	226617,3458
17	41641,68762	55158,63127	332958,3367	36284,1524	48062,03344	274679,3792
18	41641,68762	56078,31564	389036,6523	36284,1524	48863,39308	323542,7723
19	41641,68762	57013,33433	446049,9867	36284,1524	49678,11416	373220,8864
20	41641,68762	57963,94299	504013,9296	36284,1524	50506,41943	423727,3059
21	18253,59549	25832,08736	529846,017	16569,7987	23449,21513	447176,521
22	18253,59549	26262,79723	556108,8142	16569,7987	23840,19432	471016,7153
23	18253,59549	26700,68852	582809,5028	16569,7987	24237,69248	495254,4078
24	18253,59549	27145,88097	609955,3837	16569,7987	24641,8183	519896,2261
25	18253,59549	27598,49631	637553,88	16569,7987	25052,68229	544948,9084
26	18253,59549	28058,65831	665612,5383	16569,7987	25470,39679	570419,3052
27	18253,59549	28526,49279	694139,0311	16569,7987	25895,07604	596314,3812
28	18253,59549	29002,12768	723141,1588	16569,7987	26326,83615	622641,2174
29	18253,59549	29485,69305	752626,8519	16569,7987	26765,79519	649407,0126
30	18253,59549	29977,32111	782604,173	16569,7987	27212,0732	676619,0858

Figure 7.2: NPV with discounted cash flow

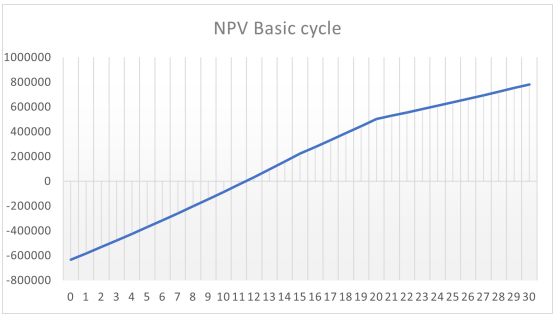

Figure 7.3: NPV for basic cycle

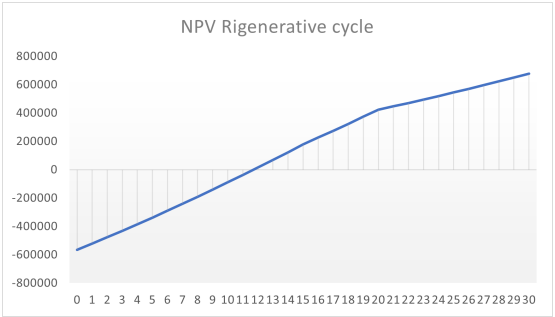

Figure 7.4: NPV for rigenerative cycle

environmental impact factor. To do this, we need to convert the data and determine the amount of environmental impact we can avoid through the use of renewable technologies. For instance, we can evaluate the amount of carbon dioxide we have prevented from being released compared to a conventional plant that generates electricity and heat using natural gas or other fuels. The table 7.6 presents significant data, highlighting how a single installed plant manages to avoid thousands of tons of carbon dioxide over its lifecycle (equivalent to a couple of dozen per year). Similarly,

Environment impact over the lifecycle				
	Parameter	**ORC base**	**ORC rigenerative**	**Unit**
TEP	Tons of equivalent Oil	647	559	t
CO2	CO_2 saved	1553	1342	t
Natural Gas	Natural gas saved	776400	671086	m^3

Table 7.6: Avoided emissions over the lifecycle

avoiding the use of alternative sources to fossil fuels, such as natural gas, which still contribute to the emission of greenhouse gases when burned in power generation plants. Furthermore, the extraction and transportation alone of a source like natural gas could result in the release of other pollutants, thus contributing to further greenhouse gas emissions.

Levelized costs				
	Parameter	**ORC base**	**ORC rigenerative**	**Unit**
LCOE	Levelized cost of electricity energy	460	410	$\$/MWh$
LCOH	Levelized cost of thermal energy	96	105	$\$/MWh$
LCOC	Levelized cost of cogenerated energy	79	84	$\$/MWh$

Table 7.7: Levelized costs for different energy output

The obtained costs show higher values for the electricity cost. Therefore, the plant is not optimized for electricity production alone, the levelized cost is high referred to as the average value with about the same discount rate($87\$/MWh$ [13]). For the plant, which is the combined production of electricity and heat, the cost of energy from cogeneration is instead very competitive.

From the future perspective, surely with the consolidation of technological development in a sector like concentrated solar power, it will be possible to further expand the profit margins from such a project. Through the use of more efficient materials and with the continuous decrease in component costs for a technology that will increasingly gain ground, it will be possible to achieve even shorter investment payback periods associated with even lower capital costs. Furthermore, beyond the potential incentives used, there is the prospect of being able to benefit from others that are more advantageous for a nation, and a continent, which will increasingly rely on renewable sources to achieve proposed objectives.

Chapter 8

Conclusion

The following document presents a thesis work that illustrates the sizing of an organic Rankine cycle for the production of both electrical and thermal energy. This is achieved through the use of solar concentrators in the form of discs, called paraboloids. The Rankine cycle is designed in both its base and regenerative cycle variants, with the addition of a heat exchanger. The solar concentrator is connected to the Rankine cycle, producing a power output of $10kW$ through the expander. This power is then converted to $9.8kW$ of electricity through the alternator while recovering useful energy in the form of heat from the exhaust steam exiting the expander. The condenser absorbs the excess energy from the exhaust steam by introducing a flow of water at an exit temperature of approximately 85 degrees Celsius. Toluene is chosen as the fluid circulating within the Rankine cycle due to its advantageous behavior under similar conditions within the cycle, despite its risks to human health. However, the environmental advantages of Toluene have been considered preferable as it circulates within the system without leaks or losses. Additionally, the installation of sensors capable of detecting potential leaks or spills has been contemplated to safeguard operators.

The behavior of each cycle component was analyzed as the reference parameters varied to determine the optimal operating point and obtain a cycle model according to the correct parameters. This analysis concluded with the determination of the cycle efficiency values in its two configurations. Although the regenerative cycle stored less recovery energy at the condenser, it proved more efficient, evidenced by its lower energy demand at the evaporator. A lower demand at the evaporator correlates with a smaller input required from the solar concentrator, resulting in a dependence on a smaller solar field. The regenerative cycle showed higher efficiency values, with an electrical efficiency of 15% and an overall plant efficiency of 79%.

In the concluding chapter, an economic analysis was conducted which showed that the two configurations exhibit contrasting aspects, with the regenerative cycle not being the most cost-effective due to lower recovery at the condenser and the presence of an additional, costly plant component. However, the investment payback period was similar for both cycles and for the base cycle, there was a net gain of over $\$700{,}000$ at the end of the cycle, thanks in part to the substantial incentives considered, net of higher initial capital investment compared to the regenerative case. Regarding environmental aspects, considering a plant lifespan of 30 years, it is evident that the use of this technology leads to the avoidance of over 1000 tonnes of CO_2 emissions into the atmosphere.

In conclusion, from an economic standpoint, it is advantageous to adopt the simple Rankine cycle, while from a thermodynamic perspective, the regenerative cycle performs better. It's also worth considering the smaller footprint of the latter, which could be advantageous for future prospects.

Although this research has made significant progress, there are still some areas that require further investigation and future development. For example, there is a need for the implementation of an energy storage system that can utilize the high temperatures achieved by the concentrator's fire. These temperatures surpass the threshold required by the operating fluid, allowing the production of electricity even during hours of solar absence. Additionally, a more in-depth study on the use of condensation water is required. This water can be utilized in various ways, including the production of domestic hot water and residential heating.

In conclusion, this thesis highlights the importance of continued research into renewable sources and the significant contribution they can make towards a more sustainable future.

Bibliography

[1] AACE International Recommended Practice No. 18R-97. Cost estimate classification system as applied in engineering, procurement, and construction for the process industries, tcm framework 7.3 , cost estimating and budgeting. Technical report, Advancement of Cost Engineering (AACE) International, 2005.

[2] International Energy Agency. Technology roadmap - a guide to development and implementation. Technical report, IEA, 2014.

[3] International Energy Agency. Energy technology perspective 2023. Technical report, IEA, 2023.

[4] Steven Lecompte Bruno Vanslambrouck Martijn Van den Broek and Michel De Paepe. Review of organic rankine cycle (orc) architectures for waste heat recovery. *Renewable and Sustainable Energy Reviews*, 2015.

[5] S Douvartzides and I Karmalis. Working fluid selection for the organic rankine cycle (orc) exhaust heat recovery of an internal combustion engine power plant. *IOP Conf. Ser.: Mater. Sci. Eng.*, 2016.

[6] D. Zhao S. Deng L. Zhao W. Xu W. Wang X. Nie e M. Chen. Overview on artificial intelligence in design of organic rankine cycle,. *Energy and AI*, 2020.

[7] D. Bhattacharyya J. Shaeiwitz W. Whiting R. Bailie e R. Turton. *Appendix A. Cost Equations and Curves for the CAPCOST Program*. Analysis, Synthesis, and Design of Chemical Processes (Fourth Edition), Prentice Hall, 2012.

[8] EIA. Levelized cost of new generation resources in the annual energy outlook 2022. *U.S. Energy Information Administration*, 2022.

[9] D. Yogi Goswami. Principle of solar engineering, third edition. Technical report, 2015.

[10] Clifford K. Ho and Andrea Ambrosini. *CHAPTER 12 THERMAL ENERGY STORAGE TECHNOLOGIES*. Sandia National Laboratories, 2022.

[11] Christiana Honsberg and Stuart Bowden. Pv education. *PV Education*.

[12] D. Yogi Goswami Elias K. Stefanakos Huijuan Chen. A review of thermodynamic cycles and working fluids for the conversion of low-grade heat. *: www.el sevier.com/locate/rser*, 2010.

[13] *Projected Costs of Generating Electricity 2020*.

[14] IEA-ETSAP IRENA. Concentrating solar power-technology brief. Technical report, IRENA, IEA-ETSAP, 2013.

[15] Johannes Sattler Bernhard Hoffschmidt Matthias GÃ¼nther Michael Joemann. *Advanced CSP Teaching Materials, Chapter 9 Thermal Energy Storage*. ENERMENA, 2011.

[16] Charles Maxwell. Cost indices. *Towering Skills*, 2024.

[17] Fabio Minchio. *Titoli di efficienza energetica: opportunitÃ per le imprese. TEE per CAR*. PhD thesis, Consorzio Energia Assindustria Vicenza, 2013.
[18] *Certificati Bianchi*.
[19] *Decreto CER*.
[20] U.S Department of Energy. Quality guidelines for energy system studies - cost estimation methodology for netl assessments of power plant performance. *National Energy Technology Laboratory*, 2011.
[21] Xingchao Wang Edward K. Levy Chunjian Pana Carlos E. Romero Carlos Rubio-Maya Lehua Pan. Working fluid selection for organic rankine cycle power generation using hot produced supercritical co2 from a geothermal reservoir. *eScolarship*, 2019.
[22] Sylvain Quoilin. *Sustainable Energy Conversion Through the Use of Organic Rankine Cycles for Waste Heat Recovery and Solar Applications*. ENERGY SYSTEMS RESEARCH UNIT AEROSPACE AND MECHANICAL ENGINEERING DEPARTMENT UNIVERSITY OF LIEGE, 2011.
[23] Vector Renewables. Solar pv power plant lifespan. *Vector Renewebals*, 2022.
[24] *Aggiornamento Mensile Certificati Bianchi*.
[25] Giuseppe Salvatore Saiana. Frequenza delle precipitazioni. *INAF Osservatorio astronomico di Palermo*, 2024.
[26] Praveen Kumar V Madhu Sharma. Analysis of heat transfer fluids in concentrated solar power (csp). *International Journal of Engineering Research & Technology (IJERT)*, 2014.
[27] SoterisA.Kalogirou. Solarthermalcollectorsandapplications. *Available online at "www.sciencedirect.com"*, 2004.
[28] Randall W. Whitesides. Process equipment cost estimating by ratio and proportion. *PDHonline Course G127*, 2020.
[29] Joakim WidÃ©n and Joakim Munkhammar. Solar radiation theory. *Research Gate*, 2019.
[30] A. Ustaoglu J. Okajima X.-R. Zhang and S. Maruyama. Assessment of a solar energy powered regenerative organic rankine cycle using compound parabolic involute concentrator. *Energy Convers. Manag., vol. 184*, 2019.
[31] Zhiqi Wang Yanhua Hu Xiaoxia Xia Qingsong Zuo Bin Zhao. Thermo-economic selection criteria of working fluid used in dual-loop orc for engine waste heat recovery by multi-objective optimization. *University of Wollongong University of Wollongong Research Online Research Online*, 2020.
[32] Ondrej Å½iÅ¾lavskÃ½. Net present value approach: method for economic assessment of innovation projects. Technical report, ScienceDirect, 2014.